THESIS

SOLUTE TRANSPORT IN VARIABLY SATURATED FLOW IN POROUS MEDIA WITH DUAL POROSITY

Submitted by

Simon A. Lorentz

Agricultural and Chemical Engineering Department

In partial fulfillment of the requirements

for the degree of Master of Science

Colorado State University

Fort Collins, Colorado

Summer 1986

COLORADO STATE UNIVERSITY

Spring, 1986

WE HEREBY RECOMMEND THAT THE THESIS PREPARED UNDER OUR SUPERVISION

BY Simon A. Lorentz

ENTITLED SOLUTE TRANSPORT IN VARIABLY SATURATED FLOW IN POROUS MEDIA WITH DUAL POROSITY

BE ACCEPTED AS FULFILLING IN PART REQUIREMENTS FOR THE DEGREE OF

Master of Science

Committee on Graduate Work

Robert C. Ward

David B. McWhorter

Adviser

Vincent G. Murphy

Department Head

ABSTRACT OF THESIS

SOLUTE TRANSPORT IN VARIABLY SATURATED FLOW IN POROUS MEDIA WITH DUAL POROSITY

The transport of chemicals through solid waste disposal piles presents a potential source of surface and groundwater contamination. In an effort to determine the scope of the potential hazard, many laboratory tests have been devised and used on the waste materials. A prerequisite for such a test would be that it yield reproducible results. An added advantage, however, would be that the mechanisms of leachate generation in the test have some resemblance to those in the field.

Therefore, on the premise that hydrodynamic conditions and solid-to-liquid ratios have a significant influence on the rate and quantities of chemical leached in situ, a standardized column leach test was developed for laboratory evaluation of oil shale solid wastes (Nazareth, 1984). In addition, an analytical model was developed to describe the effluent breakthrough curve (BTC). The physical mechanisms modelled were convection, dispersion and linear equilibrium adsorption in a partially saturated porous medium. The model predicted the results of leach tests on fine grained oil shale waste material. However, tests on large grained materials produced BTCs of a conservative chemical which were extremely asymmetric and exhibited and excessive tailing effect. This phenomenon could be caused by the diffusion of solute out of the retorted oil shale particles into the mobile water phase. The need for a model which included this additional process was realized.

An approximate model and a solution for these processes are developed in this study (Model 1). The solution is compared with another approximate model in which the diffusion process is ignored (Model 3). This comparison shows that, for a certain combination of the physical properties of the medium, the BTC can be predicted without considering the diffusion process even though the material has a significant intra-particle volume.

Model 1 predictions are compared with experimental BTC results from column leach tests. The columns are packed with selected spherical particles which have a large intra-particle volume. Different sizes of particles are used and advection rates are varied in these idealized tests. The model is also used to predict the results of BTC's resulting from tests on a retorted oil shale packed at different bulk densities.

The model successfully predicts the BTCs of leach tests where the unsaturated flow in the medium can be modelled by a Green-Ampt type wetting front. In other materials the model can be used to predict the data by calibrating the dispersion coefficient. In addition it is shown that for a specific combination of test parameters the intra-particle diffusion mechanism may be neglected even though the material has a large intra-particle volume.

Simon A. Lorentz
Agricultural and Chemical Engineering
Colorado State Univeristy
Fort Collins, CO 80523
Summer, 1986

ACKNOWLEDGMENTS

The author sincerely thanks his major professor Dr. David B. McWhorter. Dr. McWhorter's patience, encouragement and stimulating advise contributed a great deal to the success of this work. The author also expresses gratitude to his committee members Dr. Thomas G. Sanders and Dr. Robert C. Ward for their contributions during the research and during preparation of this thesis.

Sincere thanks are extended to Mr. John Brookman for his excellent construction of laboratory equipment and his precise draftmanship of the figures. The patience and cheerful cooperation of Mrs. Vicky Jensen while typing the equations is gratefully acknowledged. The author also extends sincere thanks to Mrs. Elaine Dean for typing the text and Ms. Sandy Page for typing the final draft.

The author wishes to thank his mother and family at home for their patience and support. Finally, special thanks are due to the authors wife, Yvonne and son, Andrew for their constant encouragement and patience.

Support for the research work came from the U.S. Environmental Protection Agency through Cooperative Agreement CR807668 and is gratefully acknowledged.

DEDICATION

This work is dedicated to the fond memory of my father.

TABLE OF CONTENTS

Page

APPENDICES

LIST OF TABLES

LIST OF FIGURES

LIST OF SYMBOLS

Variable	Definition	Units
a	Radius of a particle	cm
b	Half width of a fracture	cm
B	Half width of a matrix in a system of parallel fractures	cm
C	Concentration of solute in the macro-space	mg/l
C^*	Concentration of solute in the micro-space	mg/l
$\bar{C}^*$	Average concentration of solute in the micro-space	mg/l
d	Porous mdium particle diameter	cm
D	Hydrodynamic dispersion coefficient	cm^2/hr
D^*	Effective diffusion coefficient in the micro-space	cm^2/hr
D_o	Molecular diffusion coefficient	cm^2/hr
f	Fraction adsorption sites in the macro-space	
F	Diffusive flux	mg/cm^2sec
K	Volume equilibrium constant	cm^3/cm^3
K'	Constant in the isotherm $S = K'C^n$	
k_f	Mass transfer coefficient	cm/s
L	Length of a column of porous medium	cm
P	Column Peclet number, $P = vL/D$	
Pe	Peclet number, $Pe = vd/Do$	
q	Darcy flux, $v\theta$	cm/s
r	Radial dimension	cm
R	Retardation factor in the macro-space	

Variable	Definition	Units
r	Radial dimension	cm
R	Retardation factor in the macro-space	
R^*	Retardation factor in the micro-space	
S	Adsorbed solute in macro-space	mg/gm
S^*	Adsorbed solute in micro-space	mg/gm
t	time	sec
v	Darcy velocity	cm/sec
x	vertical dimension	cm
y	horizontal dimension	cm
λ	Decay constant	sec^{-1}
ϕ	Porosity of macro-space	cm^3/cm^3
ρ	Bulk density of porous medium	gm/cm^3
θ	Liquid volumetric content in the macro-space	cm^3/cm^3
θ^*	Liquid volumetric content in the micro-space	cm^3/cm^3

Chapter 1

INTRODUCTION

Many solid waste materials in the mining industry present a potential source of surface and groundwater contamination. This degradation would be caused by chemical transport in the material due to leaching by precipiation, co-disposed liquids or rising water tables.

In an effort to determine the scope of the potential hazard, many laboratory tests have been devised and used on waste materials. The value of these tests stems from the ability of the results to help in identifying the nature and quantity of chemical species expected from a given waste material subjected to given hydrologic conditions. A prerequisite for such a test would be that it yield reproducible results. An added advantage, however, would be that the mechanisms of leachate generation in the test have some resemblance to those in the field.

It was, therefore, on the premise that hydrodynamic conditions and solid-to-liquid ratios have a significant influence on the rate and quantities of chemical leached in situ, that a standardized column leach test has been developed for laboratory evaluation of oil shale solid wastes (Nazareth, 1984). The test procedure involved constant-rate, vertical injection of distilled water into a column packed with moisturized, retorted shale material. In addition, an analytical model was developed to describe the variation of the concentration of chemical species in the effluent with time. This relationship between concentration of effluent and time is known as a breakthrough curve. The physical mechanisms modelled were convection, dispersion and linear equilibrium adsorption in an unsaturated porous medium. The breakthrough curves were expressed in terms of relative concentration, C/C_I, as a function of pore volumes injected. C is the concentration in the effluent and C_I is the initial concentration in the moisturized material. The predicted breakthrough curves for nonadsorbed species were shown to pass through the point $C/C_I = 0.5$ and 1 pore volume of injected liquid. Some experimental data, however yielded asymmetric breakthrough curves in which a tailing effect was observed. In these the relative concentration was 0.5 at less than 1 total pore volume of injected water and a low, but significant, relative concentration prevailed at 1.5 to 3.0 pore volumes. This phenomenon could be caused by the dual porosity nature of the oil shale material.

The solid waste resulting from oil shale retorting processes consists of a dual porosity porous medium. Inter-particle space formed by the collection of particles in the disposal pile is termed macro-space. Intra-particle space resulting from removal of kerogen forms a micro-space. A practically stagnant solution called the immobile phase exists in the micro-space while the flowing solution or mobile phase exists in the macro-space.

It is the purpose of this study to examine the effects of a certain physical phenomenon which may cause these highly asymmetric curves. The phenomenon considered is that of diffusion of chemical solute from liquid in an immobile phase into the mobile phase. More specifically in this study:

1) An approximate model and solution are developed for the immobile/mobile phase diffusion process as well as chemical transport by dispersion and convection in the variably saturated flow;

2) The model predictions are compared with experimental results from laboratory columns packed with selected dual-porosity porous media.

The model successfully explains the differences among leaching curves resulting from varied test parameters. The study shows that for a specific combination of test parameters the immobile/mobile phase diffusion mechanism may be neglected even though the material may exhibit significant micro-space. In this case the immobile phase may be assumed to exist initially within the macro-space.

Chapter 2

LITERATURE REVIEW

A variety of different models have been developed to predict the movement of solutes through a porous media. In particular, the observation of asymmetry and tailing of breakthrough curves for nonadsorbed solutes leached through porous media has led to the development of certain models to account for these effects. Common to these models is the assumption that two distinct liquid phases exist. These are a "mobile" phase, where solute transport takes place by diffusion and convection, and an "immobile" phase, where solute is transferred to or from the mobile phase by diffusion only. Typical applications of such models can be found in the prediction of solute transport in a number of different media. These include certain solid waste products from the mining industry in which individual particles exhibit an intra-particle space resulting from the removal of a product. The immobile phase exits in the intra-particle space. Other media include aggregated soils, fractured rock and packed beds of chromatographic materials.

In some of these models adsorption and desorption processes have been considered in addition to the diffusion mechanism described. Nevertheless, all of the models have been developed using one of two basic approaches as identified by Nkedi-Kizza (1979).

In the first approach the solute transfer between mobile and immobile phases is diffusion controlled. Typically, the immobile region is assumed to have an idealized shape in order that the diffusion transfer process can be easily modelled. However, due to the uncertainty in defining the shapes and sizes of aggregates, a second approach has been widely utilized. In this approach solute transfer is modelled as a first-order exchange process. Here, the diffusive solute transfer between mobile and immobile phases is assumed to be proportional to the concentration difference between the two liquid phases. More recently, however, the first approach has been extended to include a "shape factor" which can be used to transform an analysis involving aggregates of different shapes and sizes into that for a reference particle of known geometry. (Rao, et. al., 1982; Van Genuchten, 1985).

In this chapter the two approaches are discussed separately with reference to specific models which have been documented (Sections 2.1 and 2.2). The basic differences in the assumptions adopted in developing these models are highlighted. The transport equations are described briefly and the methods of solution are summerized.

A third alternative approach has been developed by Passioura (1971). This approach is limited to a specific condition and is discussed briefly in Section 2.3. The variables used in the following sections are defined in the list of symbols.

2.1 SOLUTE TRANSFER AS AN EXCHANGE PROCESS

Much of the theoretical analyses in which the solute transfer is considered as an exchange process have followed the approach of Lapidus and Amundson (1952). These authors were interested in predicting the concentration of the inter-particle solution and the adsorbate content of the adsorbent at any time and position in a packed bed of chromatographic material. They modelled solute diffusion through the fluid in the immobile intra-particle phase and subsequent adsorption inside the particle by both a first-order and an instantaneous reaction. Longitudinal diffusion and one-dimensional convection processes were included in the analysis of the mobile phase.

The equation of mass transport in the mobile phase is given as:

$$\frac{\partial C}{\partial t} + \frac{1}{\varphi}\frac{\partial C^*}{\partial t} = D\frac{\partial^2 C}{\partial x^2} - v\frac{\partial C}{\partial x} \tag{2.1}$$

The second term represents the mass transfer between mobile and immobile phases. The first and second expressions on the right hand side describe the mobile phase dispersion and convection mechanisms. In the case of the first-order reaction process, the relationship between C* and C is given by

$$\frac{\partial C^*}{\partial t} = k_1C - k_2C^* \tag{2.2}$$

where k_1 and k_2 are constants.

The following initial and boundary conditions are imposed:

$$C(0,\ t) = Co\ (t) \tag{2.3a}$$

$$C(x,\ 0) = C_I(x) \tag{2.3b}$$

$$C^*(x,\ 0) = C^*_I(x) \tag{2.3c}$$

Equations (2.1) to (2.3a,b, and c) were solved by the method of Laplace transform. The final solution, as is typical for many of the analytical solutions, represents the solute concentration in a semi-infinite column. Despite this simplifying assumption, the solution was rather complicated to use. Coats and Smith, 1964 developed a more amenable analytical solution. These authors used a flux type inlet boundary condition as follows:

$$C - \frac{D}{v}\frac{\partial C}{\partial x} = C_o \qquad x = 0 .$$

This model was able to predict the asymmetric breakthrough data derived from tests on sandstone cores. A physical representation of the stagnant pore volume was offered by the authors. They supposed that a steady-state diffusion process took place through a narrow neck leading to the stagnant volume (Figure 2.1).

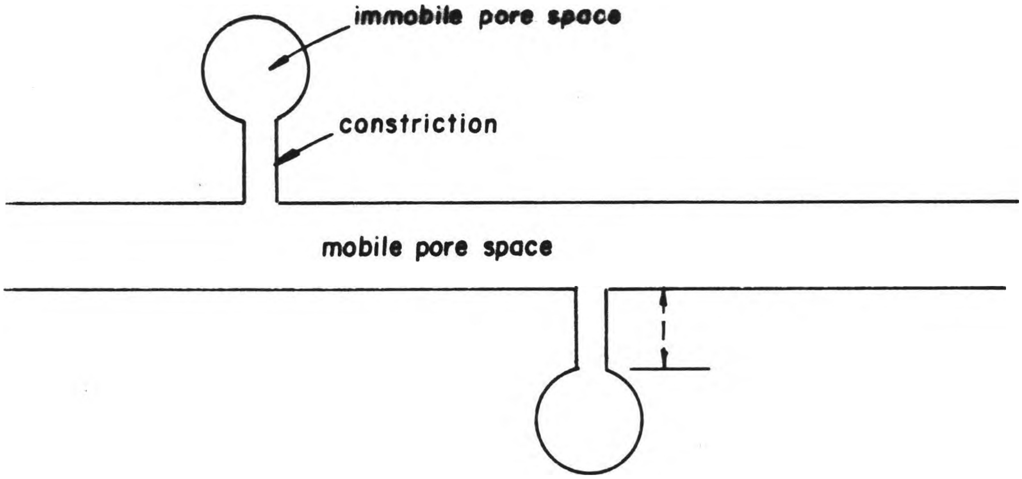

Figure 2.1. Idealized immobile pore space (Coats and Smith, 1964).

The authors argued in favor of this representation by showing that the parameter describing the length of the neck, l, was larger for the tests done on the bigger particle sandpacks than for the tests done on sandstone.

Instead of the step input described by 2.3a, Lindstrom and Narasimham (1973) have solved equations 2.1 and 2.2 for a previously distributed chemical within the porous medium.

Van Genuchten and Wierenga (1976) considered not only diffusion into the stagnant volume but also adsorption in the mobile and stagnant phases. The following transport equation was presented

$$\theta \frac{\partial C}{\partial t} + \theta^* \frac{\partial C^*}{\partial t} + f\rho \frac{\partial S}{\partial t} + (1 - f) \rho \frac{\partial S^*}{\partial t} = \theta D \frac{\partial^2 C}{\partial x^2} - \theta v \frac{\partial C}{\partial x} \quad . \tag{2.4}$$

A linear adsorption was considered such that

$$S = K'C \quad . \tag{2.5}$$

For a semi-infinite column and a pulse input of solute, the boundary and initial conditions, for a pulse period of t_1, were:

$$C - \frac{D}{v} \frac{\partial C}{\partial x} = Co \qquad 0 < t < t_1 \tag{2.6a}$$

$$= 0 \qquad t > t_1 \tag{2.6b}$$

$$C(\infty, t) = 0 \quad . \tag{2.6c}$$

Equations (2.4) to (2.6a,b and c) were solved by transforming the solution presented by Lindstrom and Narasimham (1973). In order to use this model to analyse and compare data from column leach tests, a least-squares curve fitting computer program was developed by Van Genuchten (1981). The program calculates the unknown parameters of 2.4 and 2.5 by a least squares curve fit of the data. Since verification of the conceptual processes in a model rely on measurement of all the parameters independently from the leach test data, this model has only been utilized for comparison purposes. (Nkedi-Kizza, et. al., 1983; Bryant, 1982). In these studies it was shown that the model which includes a mobile and immobile phase is able to fit data describing an asymmetric breakthrough curve; while a model which considers only the mobile phase is unable to fit these data. In addition it has been shown by Nkedi-Kizza, et. al. (1983), that the mass transfer coefficient is a function of both the physical and chemical properties of the porous medium (aggregate size, pore water velocity and solution concentration). This indicates that the mass transfer is indeed diffusion controlled.

2.2 SOLUTE TRANSFER AS A DIFFUSION PROCESS

In this approach a destinctive geometry is given to the medium containing the immobile phase. The diffusive transfer between the mobile and immobile phases is then easier to model. A number of different geometries as well as different boundary conditions and simplifying assumptions have been considered by various researchers. The simplest models involve diffusion out of (or into) an infinite matrix. These are useful in modelling solute transport in fractured rock. In another approach stagnant liquid has been equated with a finite film surrounding particles or as a finite matrix in fractured rock. A third approach consideres a finite film as well as an intraparticle stagnant region. The particle size and shape are known in this approach but the film thickness must be estimated from breakthrough curve data. A fourth approach assumes that the stagnant liquid phase exists entirely within the particle. Examples of each of these approaches are discussed in this section.

Models involving an infinite matrix have been developed by Grisak and Pickens (1980) where a finite element solution is developed and by Tang, Frind and Sudicky (1981) where the transport equations are solved analytically.

The processes considered by Tang, Frind and Sudicky (1981) are: advective transport, molecular diffusion and longitudinal mechanical dispersion in the fracture (refer to Figure 2.2); molecular diffusion from the fracture into the matrix; adsorption onto the face of the matrix and within the matrix; and radio-active decay. The equation for solute transport in the fracture is

$$\frac{\partial C}{\partial t} + \frac{v}{R}\frac{\partial C}{\partial x} - \frac{D}{R}\frac{\partial^2 C}{\partial x^2} + \lambda C + \frac{F}{bR} = 0 \qquad (2.7)$$

where R is a retardation factor, λ is a decay constant and F is the diffusive flux into (or out of) the matrix. The equation describing the transport in the matrix is

$$\frac{\partial C^*}{\partial t} - \frac{D^*}{R^*}\frac{\partial^2 C^*}{\partial y^2} + \lambda C^* = 0 \qquad b \leq y \leq \infty \qquad (2.8)$$

The diffusive flux, F is expressed by Fick's first law and is evaluated at the matrix/fracture boundary as:

$$F = -\theta D^* \left.\frac{\partial C^*}{\partial y}\right|_{y=b} \qquad (2.9)$$

Barker and Foster (1981) developed a numerical solution for solute transport in a fissure with diffusion into or out of a finite matrix.

In this model hydrodynamic dispersion was assumed to be negligable in the mobile phase (fissure). Sudicky and Frind (1982) developed an analytical solution for the case of a finite matrix. Here the initial and boundary conditions are:

$$C(x,\ 0) = 0 \qquad (2.10a)$$

$$C(0,\ t) = Co \qquad (2.10b)$$

$$C(\infty,\ t) = 0 \qquad (2.10c)$$

and

$$C^*(y,\ x,\ 0) = 0 \qquad (2.10d)$$

$$C^*(b,\ x,\ t) = C(x,\ t) \qquad (2.10e)$$

$$\frac{\partial C^*}{\partial t}(B,\ x,\ t) = 0 \qquad (2.10f)$$

where 2B is the width of the matrix. The method of solving this set of equations involved taking the Laplace transform of 2.8 and solving the ordinary differential equation. The flux, F was then expressed in Laplace space and substituted into the transformed equation 2.7. The resulting equation was solved and inverted. Much of the method of solution was extracted from Skopp and Warrick, 1974. These authors had presented a model for describing solute transfer in soils where the immobile phase was assumed to be in a film surrounding the soil particles. However, in order to simplify the solution these authors had assumed that the hydrodynamic dispersion in the mobile phase was negligible. No adsorption or decay processes were considered in this study, so that the equation describing the transport in the mobile phase was:

$$\frac{\partial C}{\partial t} + v\,\frac{\partial C}{\partial x} + \frac{D^*}{L}\left(\frac{\partial C^*}{\partial y}\right)_{y=d} = 0 \qquad (2.11)$$

and that in the immobile phase:

$$\frac{\partial C^*}{\partial t} = D^*\left(\frac{\partial^2 C^*}{\partial y^2}\right) \qquad (2.12)$$

where d was the thickness of the immobile film and L was the width of the mobile phase. A schematic representation of the simplified model of the porous media is shown in Figure 2.3.

Solutions for solute transport in porous media where the immobile phase is assumed to exist entirely within spherical particles have been presented by Rasmuson and Neretnieks, 1980 and Van Genuchten, 1985. The general equation describing solute transport in the macro space is given as

$$\frac{\partial C}{\partial t} + \frac{\theta^*}{\theta}\,\frac{\partial \overline{C^*}}{\partial t} = D\,\frac{\partial^2 C}{\partial x^2} - v\,\frac{\partial C}{\partial x} \qquad (2.13)$$

where $\overline{C^*}$ is defined as the average concentration of the immobile phase. For spherical particles this is given by

$$\overline{C^*}\,(x,\ t) = \frac{3}{a^2}\int_0^a r^2 C^*\,(x,\ r,\ t)\ dv \qquad (2.14)$$

where C^* is the local concentration within the sphere and a the radius of the sphere. The transport of solute within the sphere is described by

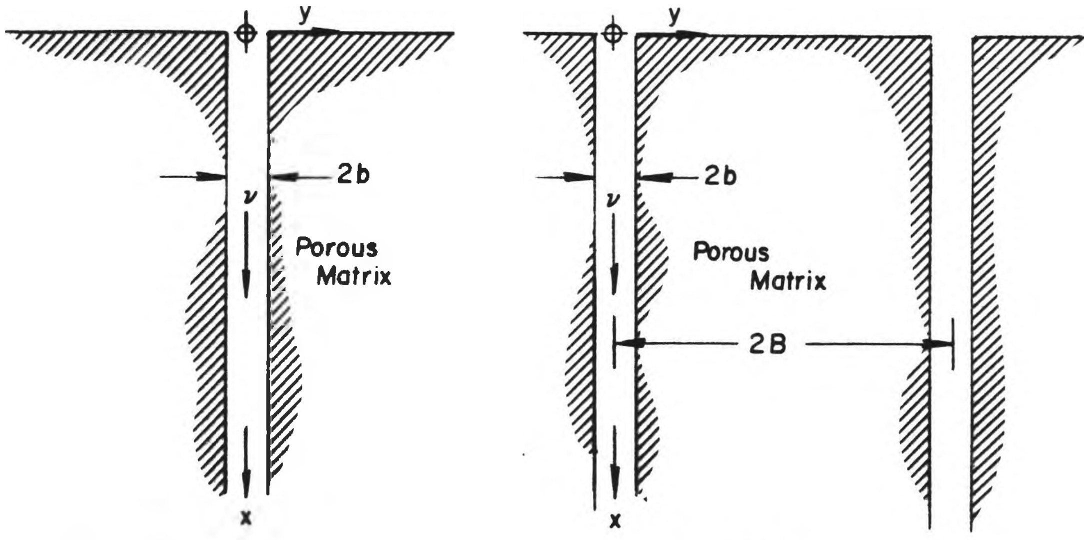

Infinite Matrix
(Tang et al 1981)

Finite Matrix
(Sudicky et al 1982)

Figure 2.2. Idealized fracture-matrix systems.

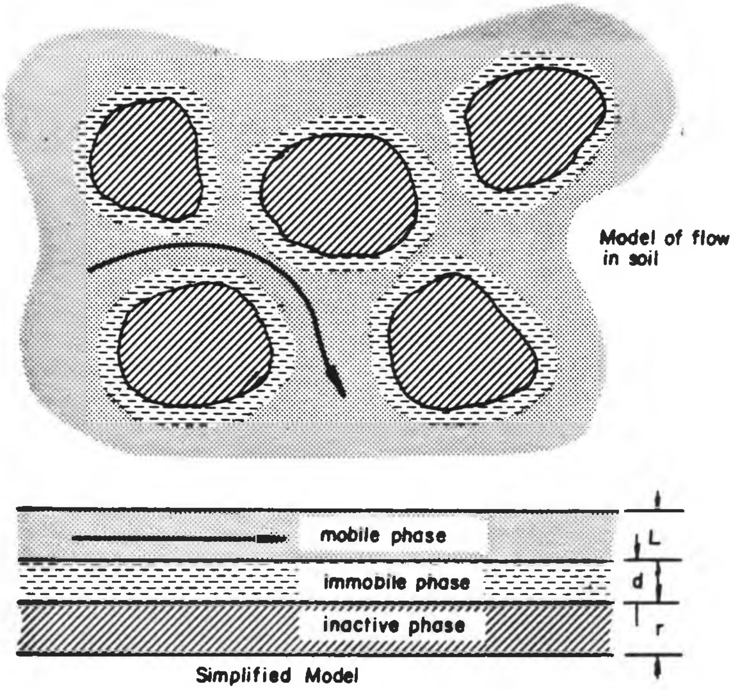

Figure 2.3. Idealized flow regime in porous media (Skopp and Warrick, 1974).

$$R^* \frac{\partial C^*}{\partial t} = \frac{D^*}{r^2} \frac{\partial}{\partial r} \left(r^2 \frac{\partial C^*}{\partial r}\right) \quad . \tag{2.15}$$

Van Genuchten, 1985 presents a solution for the volume averaged concentration within a column using flux type inlet boundary conditions. The condition linking equations 2.13 and 2.15 is:

$$C(x,\ t) = C^*(x,\ a,\ t) \tag{2.16}$$

which requires that the concentrations are continuous at the macropore walls.

A solution to predict effluent curves from a finite system is solved for flux-averaged concentrations by Rasmuson and Neretnieks, 1980. However, the continuity condition considered, requires that. the mass entering or leaving the spherical particles must equal the mass transported across a stagnant fluid film of width b at the external surface. The continuity condition is, therefore:

$$\frac{\partial \overline{C^*}}{\partial t} = \frac{3k_f}{b} \left(C - \frac{C^*(x,\ a,\ t)}{K}\right) \tag{2.17}$$

where k_f is a mass transfer coefficient and K is a volume equilibrium constant.

Van Genuchten, 1985 has presented a solution for the flux-averaged concentration similar to Rasmuson and Neretnieks but with the simpler continuity condition 2.16. This solution is presented in detail in Chapter 3. Shape factors for the conversion of various aggregate geometries into equivalent spherical sizes have been developed by Van Genuchten, 1985 and Roa, et. al., 1982.

2.3 INCLUSION OF MICRO-SPACE DIFFUSION INTO DISPERSION COEFFICIENT

Passioura (1971) showed that, for certain conditions the radial diffusion into or out of the micro-space or immobile phase could be considered as an additional contribution to the dispersion coefficient. This author derived the following expression for, the hydrodynamic dispersion coefficient.

$$D/D_o = k_2 + k_3(Pe) + k_4(Pe)^2$$

where $k_2 = \{\phi/(\phi^* + \phi)\}\{D_m/D_o\}$

$k_3 = \frac{1}{2}$

$k_4 = \{\phi^* D_o\}/\{60\phi D^*\}$

ϕ^* = microporosity

ϕ = macroporosity

D^* = effective diffusion coefficient of solute in the micro-space

D_m = effective diffusion coefficient of solute in the macro-space

D_o = molecular diffusion coefficient.

The condition for which this approach is valid is

$$Pe < 13.3\{D^*/D_o\}\{\phi^*/(\theta + \theta^*)\}\{L/d\}$$

where $Pe = \frac{vd}{D_o}$

and v = darcy velocity,

d = mean particle size,

L = column length.

2.4 SOLUTE TRANSPORT IN UNSATURATED POROUS MEDIA

All the models discussed in 2.1 and 2.2 have been derived assumming a constant liquid content. These solutions are therefore only valid for saturated flow or for conditions where a Green-Ampt type wetting front is assumed.

Nazareth, 1984, following an analysis of Wilson and Gelhar, 1981, presented a solution for solute transport in an unsaturated porous medium which accounts for varying liquid content. However, the transport equation does not account for the diffusion from an immobile phase. The equation describing the solute transport is:

$$(\Theta + \rho_b k_d) \frac{\partial C}{\partial t} = \frac{\partial}{\partial x} (\Theta D \frac{\partial C}{\partial x}) - q\frac{\partial C}{\partial x} .$$

A moving coordinate system is introduced by applying the method of characteristics to the equation describing only convection of the solute. This technique will be used later in Chapter 3 although the problem will be simplified by assumming a Green-Ampt wetting front.

Chapter 3

THEORETICAL DEVELOPMENT

A number of different models which consider diffusion of solute from a stagnant phase into a mobile phase (or vice-versa) in porous media or fractured rock have been discussed in Chapter 2. In this chapter specific models are developed and analytical solutions are derived for the transport of solute through a column of porous media. In these models solute is assumed to be transported in the mobile phase which exists in the void space between uniformly sized, spherical particles. In addition, these particles are assumed to be made up of a closely packed matrix of solid elements and thus exhibit a "microporosity". In two of the models developed or described here, a diffusion process is used to describe the transport of solute out of the practically stagnant solution in the micropores into the mobile phase in the macropores (and vice-versa). In each model a Green-Ampt type wetting front is assumed to describe the volumetric solution content in the macropores.

Three models are presented in order to show the significance of various assumptions. The first model is formulated from basic mass balance principles and the derivation of the solution is shown in detail.

The second model is similar to the first except that the mass flux into or out of the micropores is formulated differently. A boundary condition on the macropore solution is also different to the first solution (Van Genuchten, 1985).

In the third model the transport of the micropore solute is not described as a diffusion process. Instead the micropore solute is assumed to exist initially within the macropores. This initial solution then advances ahead of the invading solution. Even though a micropore diffusion process is not considered, it will be shown that this model is valuable for certain cases when describing solute transport in porous media which do exhibit microporosity.

3.1 MODEL 1

In this model the convective-dispersion equation is firstly derived from mass balance principles. The solution strategy is described and then the derivation of the solution is shown in detail. Finally the method of evaluating the solution is described.

3.1.1 The convective-dispersion equation

The convective-dispersion equation is derived by applying the law of conservation of mass. It is assumed that the porous medium consists of spherical particles of uniform size and that these particles are made up of a closely packed matrix of solid elements.

Consider the mass flux into and out of a small elemental volume of porous medium (Figure 3.1). The mass flux will be considered in one direction only.

The mass balance can be represented by:

$$- (\theta J + \frac{\partial(\theta J)}{\partial x} dx)dydz + \theta J dydz + F_m = \frac{\partial M}{\partial t}$$

or $$-\frac{\partial(\theta J)}{\partial x}\,dxdydz + F_m = \frac{\partial M}{\partial t}\,. \qquad (1)$$

where J = mass flux of solute on the liquid filled cross-section of macropore space

F_m = mass flux from the micropore solution into the macropore space (positive when mass is being added to the macropore solution)

M = total mass of chemical in the macropore solution of the elemental volume of porous medium, or

$$= Cdxdydz\theta \qquad (2)$$

where C = mass of dissolved chemical per unit volume of macropore solution

and θ = volume of macropore solution per unit volume of porous medium.

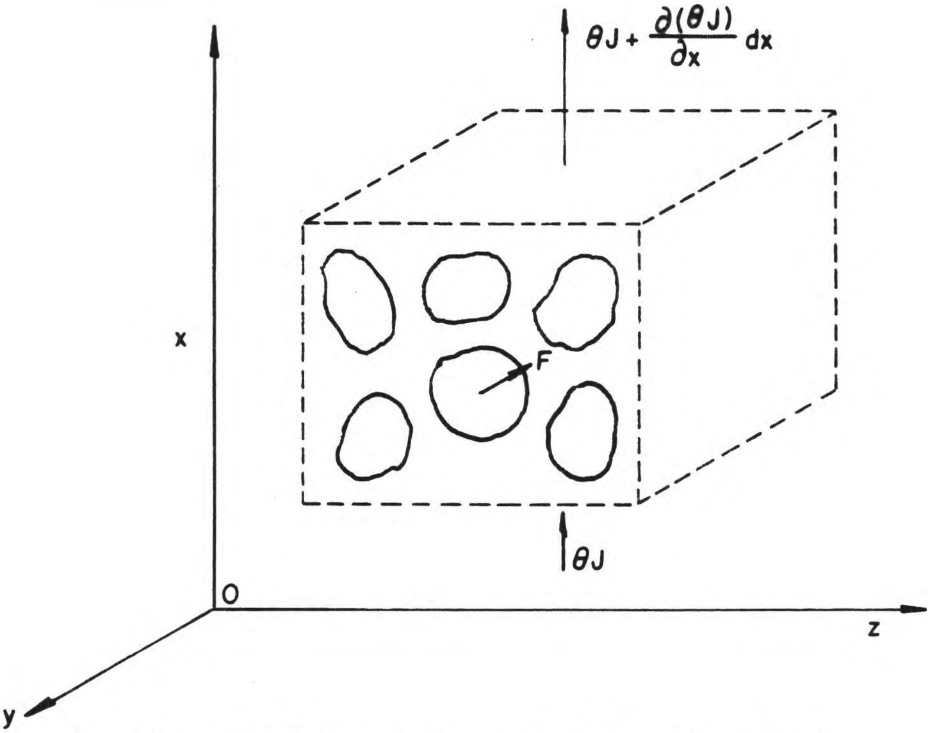

Figure 3.1. One-dimensional mass balance in elemental volume.

Also $$J = -D \frac{\partial C}{\partial x} + vC \qquad (3)$$

where D = coefficient of hydrodynamic dispersion

and v = seepage velocity and is equal to q/θ.

The mass flux in the elemental volume of porous medium due to diffusion out of the micropores of the spherical particles can be obtained by first considering the mass flux at the surface of one sphere.

$$F_s = -D^* \left.\frac{\partial C^*}{\partial r}\right|_{r=a} \theta' \; 4\pi a^2 \qquad (4)$$

where C^* = mass of dissolved chemical per unit volume of micropore solution.

$D^* = D_o/\tau^2$ where τ^2 is the tortuosity in the spherical particle and D_o is the molecular diffusion coefficient.

θ' is defined as the ratio of the volume of micropore solution to the volume of the sphere. This can also be defined as the ratio of surface area of micropore solution to the surface area of a sphere.

Now

$$\theta' = \frac{\theta^*}{1 - \phi_m} ,$$

where $$\phi_m = \frac{\text{volume of macropores}}{\text{volume of porous medium}}$$

and $$\theta^* = \frac{\text{volume of micropore solution}}{\text{volume of porous medium}} .$$

Therefore, (4) can be rewritten as

$$F_s = -D^* \left.\frac{\partial C^*}{\partial r}\right|_{r=a} \frac{\theta^*}{1 - \phi_m} 4\pi a^2 . \qquad (5)$$

Noting that the number of spheres per volume element is:

$$\frac{1-\phi_m}{\frac{4}{3}\pi a^3}\, dxdydz\ , \tag{6}$$

the total mass flux due to micropore diffusion can now be written as

$$F_m = -D^* \left.\frac{\partial C^*}{\partial r}\right|_{r=a} .3\, \frac{\theta^*}{a}\, dxdydz\ . \tag{7}$$

Expressions (2), (3) and (7) can be substituted into (1) to give:

$$\left\{\frac{\partial}{\partial x}\left(\theta D\frac{\partial C}{\partial x}\right) - \frac{\partial}{\partial x}(\theta v C)\right\} dxdydz - \frac{3\theta^*}{a} D^* \left.\frac{\partial C^*}{\partial r}\right|_{r=a} dxdydz = \frac{\partial(\theta C)}{\partial t}\, dxdydz. \tag{8}$$

By assuming a Green-Ampt wetting front and steady flow, θ, D and v become constants so Eq. (8) reduces to:

$$\frac{\partial C}{\partial t} = D\,\frac{\partial^2 C}{\partial x^2} - v\,\frac{\partial C}{\partial x} - \frac{3\theta^*}{a\theta} D^* \left.\frac{\partial C^*}{\partial r}\right|_{r=a} . \tag{9}$$

By defining a variable, s as:

$$s = \frac{3\theta^*}{a}\ , \tag{10}$$

equations (11), (12) and (13) can now be written to describe the diffusion in the spherical particles and the convective-dispersion process for flow in the macropore space.

The equation describing the diffusion in the spherical particles is (Carlslaw and Jaeger, 1959):

$$\frac{\partial C^*}{\partial t} = D^* \left(\frac{\partial^2 C^*}{\partial r^2} + \frac{2}{r}\,\frac{\partial C^*}{\partial r}\right) \tag{11}$$

with boundary and initial conditions

$$C^*(x, r, 0) = Cm \tag{11a}$$

$$\frac{\partial C^*}{\partial r}(x, 0, t) = 0 \tag{11b}$$

$$C^*(x, a, t) = C(x, t) \tag{11c}$$

The last condition requires that concentrations in the micro- and macropores are continuous at the surface of the spheres. The equation describing the transport in the macro-space behind the wetting front is:

$$\frac{\partial C}{\partial t} = D \frac{\partial^2 C}{\partial x^2} - v \frac{\partial C}{\partial x} + \frac{s}{\theta} G^* \tag{12}$$

where G^* is defined as:

$$G^* = - D^* \frac{\partial C^*}{\partial r}\Big|_{r=a} \tag{13}$$

It is assumed that Eq. (12) could be written in the same form if C was defined as flux averaged concentrations (Parker et al., 1984; Rasmuson et al., 1980 and De Smedt et al., 1979). The initial and boundary conditions can then be written as:

$$C(x, 0) = Cm \tag{12a}$$

$$C(0, t) = Co \tag{12b}$$

$$C(\infty, t) = Cm \tag{12c}$$

The solution of this linked pair of equations is made easier by converting the concentrations to the forms:

$$c = (C - Cm)/(Co - Cm).$$

and $$c^* = r(C^* - Cm) / (C_o - Cm).$$

The equations for the micro- and macro-space can now be rewritten as:

$$\frac{\partial c^*}{\partial t} = D^* \frac{\partial^2 c^*}{\partial r^2} \qquad \text{(micro-space)} \qquad (14)$$

$$c^*(x, r, 0) = 0 \qquad (14a)$$

$$c^*(x, 0, t) = 0 \qquad (14b)$$

$$c^*(x, a, t) = ac(x, t) \qquad (14c)$$

$$\frac{\partial c}{\partial t} = D \frac{\partial^2 c}{\partial x^2} - v \frac{\partial c}{\partial x} + \frac{s}{\theta} J^* \left(\frac{1}{Co - Cm}\right) \qquad \text{(macro-space)} \qquad (15)$$

$$c(x, 0) = 0 \qquad (15a)$$

$$c(0, t) = 1 \qquad (15b)$$

$$c(\infty, t) = 0 \qquad (15c)$$

$$J^* = -D^* \left(\frac{Co - Cm}{a}\right) \left(\frac{\partial c^*}{\partial r} - \frac{1}{a} c^*\right)\bigg|_{r=a} . \qquad (16)$$

3.1.2 Solution strategy

The solution strategy for Eqs. (14) to (16) is as follows:

a. Apply the Laplace transform to (14), solve the ordinary differential equation and express the concentration gradient at the surface of the sphere in terms of its Laplace transform.

b. Apply the Laplace transform to (16) and substitute the transformed interface gradient from step a. Substitute this into the transformed form of (15).

c. Solve the resulting ordinary differential equation.

d. Invert the solution.

3.1.3 Derivation of the solution

Taking the Laplace transform of (14) with respect to t yields

$$\sigma \bar{c}^* - 0 = D^* \frac{d^2 \bar{c}^*}{d\, r^2} \tag{17}$$

$$\bar{c}^*(x,\ 0,\ \sigma) = 0 \tag{17a}$$

$$\bar{c}^*(x,\ a,\ \sigma) = a\bar{c}(x,\ \sigma) \tag{17b}$$

where $\bar{c}^*$ is the Laplace transform of c^* and σ is the transformed variable, t.

Assuming a solution of the form:

$$\bar{c}^* = A \sinh r \sqrt{\frac{\sigma}{D^*}} + B \sinh \left(\sqrt{\frac{\sigma}{D^*}} (a - r)\right)$$

and applying (17a) yields $B = 0$.

Applying (17b) yields $A = \dfrac{a\bar{c}(x,\ \sigma)}{\sinh a \sqrt{\frac{\sigma}{D^*}}}$

$$\text{so} \quad \bar{c}^* = a\bar{c}\ .\ \frac{\sinh r \sqrt{\frac{\sigma}{D^*}}}{\sinh a \sqrt{\frac{\sigma}{D^*}}} \tag{18}$$

It is convenient to express the mass flux at the boundary in the Laplace transform space. Equation (16) transforms to:

$$\bar{J}* = -D* \frac{(Co - Cm)}{a} \left(\frac{d\bar{c}*}{dr} - \frac{1}{a}\bar{c}*\right)\Bigg|_{r=a} . \tag{19}$$

Differentiating (18) and substituting into (19) the transformed flux becomes

$$\bar{J}* = -D*\left(\frac{Co - Cm}{a}\right) \left\{ a\bar{c} \left(\sqrt{\frac{\sigma}{D*}} \frac{\cosh r\sqrt{\frac{\sigma}{D*}}}{\sinh a\sqrt{\frac{\sigma}{D*}}} - \frac{1}{a} \frac{\sinh r\sqrt{\frac{\sigma}{D*}}}{\sinh a\sqrt{\frac{\sigma}{D*}}} \right) \Bigg|_{r=a} \right\} . \tag{20}$$

Evaluating (20) at r = a yields:

$$\bar{J}* = -D* \ (Co - Cm) \cdot \left(\sqrt{\frac{\sigma}{D*}} \coth a\sqrt{\frac{\sigma}{D*}} - \frac{1}{a}\right) \bar{c}. \tag{21}$$

Now taking the Laplace transform of (15) and substituting (21) gives:

$$\frac{d^2\bar{c}}{dx^2} - \frac{v}{D}\frac{d\bar{c}}{dx} - \left\{\frac{sD*}{\theta D}\left(\sqrt{\frac{\sigma}{D*}} \coth a\sqrt{\frac{\sigma}{D*}} - \frac{1}{a}\right) + \frac{\sigma}{D}\right\}\bar{c} = 0 \tag{22}$$

$$\bar{c}(0,\ \sigma) = 1/\sigma \tag{22a}$$

$$\bar{c}(\infty,\ t) = 0, \tag{22b}$$

where $\bar{c}$ is the Laplace transform of c. Eq. (22) has a solution of the form

$$\bar{c} = A\exp(w\ x_{+}) + B\exp(w\ x_{-}) \tag{23}$$

where $$w_{\pm} = \frac{V}{2D} \pm \frac{1}{2} \left\{ \frac{V^2}{D^2} + \left[\frac{4sD^*}{\theta D} \left(\sqrt{\frac{\sigma}{D^*}} \coth a \sqrt{\frac{\sigma}{D^*}} - \frac{1}{a} \right) + \frac{4\sigma}{D} \right] \right\}^{1/2} . \tag{24}$$

Because the boundary condition (22b) requires that the solution remain bounded, the constant A in (23) must be 0. The constant B is evaluated from the condition (22a). Applying this condition to (23) yields:

$$B = 1/\sigma. \tag{25}$$

Thus, Eq. (23) becomes:

$$\bar{c} = \frac{1}{\sigma} \exp\left\{ \left[\frac{V}{2D} - \frac{1}{2} \left(\frac{V^2}{D^2} + \left[\frac{4sD^*}{\theta D} \left(\sqrt{\frac{\sigma}{D^*}} \coth a \sqrt{\frac{\sigma}{D^*}} - \frac{1}{a} \right) + \frac{4\sigma}{D} \right] \right)^{1/2} \right] x \right\} . \tag{26}$$

Inversion of the right hand side of (26) is difficult due to the square root in the exponential argument. The following identity can be used to simplify the inversion (Gradshteyn and Ryzhik, 1980).

$$\int_0^\infty \exp\left(-\xi^2 - \frac{x^2}{\xi^2}\right) d\xi = \frac{\pi^{1/2}}{2} \exp(-2x) \tag{27}$$

Using (27), Eq. (26) becomes

$$\bar{c} = \frac{2}{\sigma \pi^{1/2}} \exp\left(\frac{VX}{2D}\right) \cdot$$

$$\cdot \int_0^\infty \exp\left[-\xi^2 - \frac{x^2}{4\xi^2} \left\{ \left(\frac{V}{2D}\right)^2 + \frac{sD^*}{\theta D} \left(\sqrt{\frac{\sigma}{D^*}} \coth a \sqrt{\frac{\sigma}{D^*}} - \frac{1}{a} \right) + \frac{\sigma}{D} \right\} \right] d\xi . \tag{28}$$

Eq. (28) can also be written as:

$$\bar{c} = \frac{2}{\pi^{1/2}} \exp\left(\frac{VX}{2D}\right) \int_0^\infty \exp\left[-\xi^2 - \frac{1}{4\xi^2}\left(\frac{VX}{2D}\right)^2 + \frac{1}{4\xi^2}\left(\frac{sD^* x^2}{\theta Da}\right)\right] \cdot$$

$$\frac{1}{\sigma} \exp\left[-\frac{x^2\sigma}{4\xi^2 D}\right] \cdot \exp\left[-\frac{x^2 sD^*}{4\xi^2 \theta D}\left(\sqrt{\frac{\sigma}{D^*}} \coth a \sqrt{\frac{\sigma}{D^*}}\right)\right] d\xi. \tag{29}$$

The dimensionless concentration can be written in terms of the convolution integral of the transforms of the two expressions:

$$\frac{1}{\sigma} \exp\left[-\frac{x^2\sigma}{4\xi^2 D}\right] \tag{30}$$

and

$$\exp\left[-\frac{x^2 sD^*}{4\xi^2 \theta D}\left(\sqrt{\frac{\sigma}{D^*}} \coth a \sqrt{\frac{\sigma}{D^*}}\right)\right] . \tag{31}$$

It is noted that the inverse Laplace transform of (30) is simply the step function, therefore:

$$L^{-1}\left\{ \frac{1}{\sigma} \exp\left[\frac{-x^2\sigma}{4\xi^2 D}\right]\right\} = H\left(t - \frac{x^2}{4\xi^2 D}\right) = 1 \quad t > \frac{x^2}{4\xi^2 D} \tag{32}$$

$$= 0 \quad t < \frac{x^2}{4\xi^2 D} .$$

The inverse Laplace transform of (29) can now be written as

$$c = \frac{2}{\pi^{1/2}} \exp\left(\frac{P}{2}\right) \int_0^\infty \exp\left[-\xi^2 - \frac{1}{4\xi^2}\left(\left(\frac{P}{2}\right)^2 - \frac{\gamma}{a}\right)\right] \cdot$$

$$\int_0^T L^{-1}\left\{\exp\left[- \frac{\gamma}{4\xi^2}\left(\sqrt{\frac{\sigma}{D^*}} \coth a \sqrt{\frac{\sigma}{D^*}}\right)\right]\right\}_\tau d\tau , \tag{33}$$

where $$P = \frac{vx}{D} \tag{34}$$

$$\gamma = \frac{x^2 sD^*}{\theta D} \tag{35}$$

$$T = t - \frac{x^2}{4\xi^2 D} \quad T \geq 0 . \tag{36}$$

It is now required to find the inverse Laplace transform of:

$$\exp\left[- \frac{\gamma}{4\xi^2} \left(\sqrt{\frac{\sigma}{D^*}} \coth a \sqrt{\frac{\sigma}{D^*}} \right) \right] \tag{37}$$

The inverse of an expression similar to (37) has been evaluated by Skopp and Warwick (1974). Their expression contained the hyperbolic tangent where (37) contains the hyperbolic cotangent. The inverse transform is evaluated as a contour integral along the imaginary axis as follows:

$$L^{-1} \{\exp - \left[\frac{\gamma}{4\xi^2} \left(\sqrt{\frac{\sigma}{D^*}} \coth a \sqrt{\frac{\sigma}{D^*}} \right) \right] \} =$$

$$\frac{1}{2\pi i} \int_{-i\infty}^{i\infty} \exp(\sigma\tau) \exp(\frac{\gamma}{4\xi^2} \sqrt{\frac{\sigma}{D^*}} \coth a \sqrt{\frac{\sigma}{D^*}}) \, d\sigma . \tag{38}$$

Making the substitutions:

$\sigma = i\mu^2/2$ on the negative imaginary axis and

$\sigma = i\lambda^2/2$ on the positive imaginary axis gives:

$$L^{-1} = \frac{1}{2\pi} \int_0^\infty \lambda \exp\left\{ \frac{i\lambda^2\tau}{2} - \frac{\gamma}{4\xi^2 \sqrt{D*}} \left(\frac{i+1}{2}\right) \lambda \coth\left[\frac{a}{\sqrt{D*}} \left(\frac{i+1}{2}\right) \lambda \right] \right\} d\lambda$$

$$+ \frac{1}{2\pi} \int_0^\infty \mu \exp\left\{ \frac{-i\mu^2\tau}{2} - \frac{\gamma}{4\xi^2 \sqrt{D*}} i\left(\frac{i+1}{2}\right) \mu \coth\left[\frac{a}{\sqrt{D*}} i\left(\frac{i+1}{2}\right) \mu \right] \right\} d\mu \, . \qquad (39)$$

Consider the first integral in (39) together with the following identity (Dwight, 1961)

$$\coth\left\{\beta \left(\frac{i+1}{2}\right) \lambda\right\} = \frac{\sinh \beta\lambda - i \sin \beta\lambda}{\cosh \beta\lambda - \cos \beta\lambda} \, . \qquad (40)$$

Thus, the first integral of the right hand side of (39) in which (40) has been used becomes:

$$\int_0^\infty \lambda \exp\left\{ \frac{i\lambda^2\tau}{2} - \frac{\gamma}{4\xi^2 \sqrt{D*}} \left(\frac{i+1}{2}\right) \lambda \coth\left[\frac{a}{\sqrt{D*}} \left(\frac{i+1}{2}\right) \lambda \right] \right\} d\lambda =$$

$$\int_0^\infty \lambda \exp\left\{ \frac{i\lambda^2\tau}{2} - \frac{\gamma}{4\xi^2 \sqrt{D*}} \left(\frac{i+1}{2}\right) \lambda \left[\frac{\sinh \frac{a}{\sqrt{D*}} \lambda - i\sin \frac{a}{\sqrt{D*}} \lambda}{\cosh \frac{a}{\sqrt{D*}} \lambda - \cos \frac{a}{\sqrt{D*}} \lambda} \right] \right\} d\lambda. \qquad (41)$$

The real and imaginary parts in the right hand side of (41) can be separated by defining:

$$\lambda_R = - \frac{\gamma}{4\xi^2 \sqrt{D*}} \cdot \frac{\lambda}{2} \cdot \left[\frac{\sinh \frac{a}{\sqrt{D*}} \lambda + \sin \frac{a}{\sqrt{D*}} \lambda}{\cosh \frac{a}{\sqrt{D*}} \lambda - \cos \frac{a}{\sqrt{D*}} \lambda} \right] \qquad (42)$$

and

$$\lambda_I = \frac{\lambda^2\tau}{2} - \frac{\gamma}{4\xi^2 \sqrt{D*}} \cdot \frac{\lambda}{2} \cdot \left[\frac{\sinh \frac{a}{\sqrt{D*}} \lambda - \sin \frac{a}{\sqrt{D*}} \lambda}{\cosh \frac{a}{\sqrt{D*}} \lambda - \cos \frac{a}{\sqrt{D*}} \lambda} \right] \qquad (43)$$

The right hand side of (41) can now be written as:

$$\int_0^\infty \lambda \exp(\lambda_R + i\lambda_I)\, d\lambda \tag{44}$$

which can be written as:

$$\int_0^\infty \lambda \exp\left[\lambda_R\right] (\cos \lambda_I + i\sin \lambda_I)\, d\lambda \tag{45}$$

Similarly, the second integral of (39) results in the conjugate of (45). Thus, subtracting out the imaginary parts gives, for the right hand side of (39):

$$L^{-1} = \frac{1}{\pi} \int_0^\infty \lambda \exp \lambda_R \cos \lambda_I \, d\lambda \ . \tag{46}$$

Using this expression in (33) yields:

$$c = \frac{2}{\pi^{3/2}} \exp(\tfrac{P}{2}) \int_0^\infty \exp\left[-\xi^2 - \frac{1}{4\xi^2}((\tfrac{P}{2})^2 - \tfrac{\gamma}{a})\right] \int_0^T \int_0^\infty \lambda.\exp.\lambda_R.\cos\lambda_I.d\lambda d\tau d\xi \ . \tag{47}$$

The order of the two inner integrals can be interchanged and the integration with respect to τ can be carried out, giving:

$$c = \frac{4}{\pi^{3/2}} \exp(\tfrac{P}{2}) \int_0^\infty \exp\left[-\xi^2 - \frac{1}{4\xi^2} ((\tfrac{P}{2})^2 - \tfrac{\gamma}{a}) \right] .$$

$$\int_0^\infty \exp\left[- \frac{\gamma}{4\xi^2 \sqrt{D^*}} \frac{\lambda}{2} \frac{\sinh \frac{a}{\sqrt{D^*}} \lambda + \sin \frac{a}{\sqrt{D^*}} \lambda}{\cosh \frac{a}{\sqrt{D^*}} \lambda - \cos \frac{a}{\sqrt{D^*}} \lambda} \right] .$$

$$\left\{\sin\left[\frac{T\lambda^2}{2} - \frac{\gamma}{4\xi^2\sqrt{D^*}}\,\frac{\lambda}{2}\,\frac{\sinh\frac{a}{\sqrt{D^*}}\lambda - \sin\frac{a}{\sqrt{D^*}}\lambda}{\cosh\frac{a}{\sqrt{D^*}}\lambda - \cos\frac{a}{\sqrt{D^*}}\lambda}\right]\right.$$

$$\left.-\sin\left[-\frac{\gamma}{4\xi^2\sqrt{D^*}}\,\frac{\lambda}{2}\,\frac{\sinh\frac{a}{\sqrt{D^*}}\lambda - \sin\frac{a}{\sqrt{D^*}}\lambda}{\cosh\frac{a}{\sqrt{D^*}}\lambda - \cos\frac{a}{\sqrt{D^*}}\lambda}\right]\right\}\frac{d\lambda}{\lambda}\,d\xi \quad . \qquad (48)$$

In Eq. (48) it is required that

$$t \geq \frac{x^2}{4\xi^2 D}$$

or $\xi \geq \frac{x}{2}\sqrt{\frac{1}{tD}}$.

Also recalling that $c = \left(\frac{C - Cm}{Co - Cm}\right)$, the final form of the relative concentration at x = L is:

$$\frac{C}{Cm} = \left(\frac{Co}{Cm} - 1\right)\frac{4}{\pi^{3/2}}\exp\left(\frac{P}{2}\right)\int^{\infty}\exp\left[-\xi^2 - \frac{1}{4\xi^2}\left(\left(\frac{P}{2}\right)^2 - \frac{\gamma}{a}\right)\right] .$$

$$\int_0^{\infty}\exp\left[-\frac{\gamma}{4\xi^2\sqrt{D^*}}\,\frac{\lambda}{2}\,\frac{\sinh\frac{a}{\sqrt{D^*}}\lambda + \sin\frac{a}{\sqrt{D^*}}\lambda}{\cosh\frac{a}{\sqrt{D^*}}\lambda - \cos\frac{a}{\sqrt{D^*}}\lambda}\right] .$$

$$\left\{\sin\left[\frac{T\lambda^2}{2} - \frac{\gamma}{4\xi^2\sqrt{D^*}}\,\frac{\lambda}{2}\left(\frac{\sinh\frac{a}{\sqrt{D^*}}\lambda - \sin\frac{a}{\sqrt{D^*}}\lambda}{\cosh\frac{a}{\sqrt{D^*}}\lambda - \cos\frac{a}{\sqrt{D^*}}\lambda}\right)\right]\right.$$

$$\left.-\sin\left[-\frac{\gamma}{4\xi^2\sqrt{D^*}}\,\frac{\lambda}{2}\left(\frac{\sinh\frac{a}{\sqrt{D^*}}\lambda - \sin\frac{a}{\sqrt{D^*}}\lambda}{\cosh\frac{a}{\sqrt{D^*}}\lambda - \cos\frac{a}{\sqrt{D^*}}\lambda}\right)\right]\right\}\frac{d\lambda}{\lambda}\,d\xi + 1 \qquad (49)$$

where $P = \frac{vL}{D}$ (50)

$$\gamma = \frac{L^2 sD^*}{\theta D} \qquad (51)$$

$$s = \frac{3\theta^*}{a} \qquad (52)$$

$$T = t - \frac{L^2}{4\xi^2 D}, \qquad T \geq 0 \qquad (53a)$$

and $\xi \geq \frac{L}{2}\sqrt{\frac{1}{tD}}$. (53b)

3.1.4 Evaluation of the solution

The double integral describing the relative concentration, C/Cm was evaluated using a Trapezoidal rule numerical integration procedure. An IBM XT microcomputer was used to execute the program which was written in Fortran 77. The computer program used to evaluate the integrals is listed in Appendix B1. In a sample printout the breakthrough curve has been expressed as actual concentration versus time as well as relative concentration versus pore volumes, PV, where:

$$PV = \frac{v\theta t}{(\theta + \theta^*)L} .$$

3.2 MODEL 2

The second model has been presented by Van Genuchten (1985). The equation describing the transport in the macropore system is:

$$\theta R \frac{\partial C}{\partial t} + \theta^* R^* \frac{\partial C_{im}}{\partial t} = \theta D \frac{\partial^2 C}{\partial x^2} - \theta v \frac{\partial C}{\partial x} . \qquad (54)$$

where R and R* are the retardation factors in the mobile and immobile regions respectively.

C_{im} is the flux averaged solution concentration in the spherical particles. This concept of considering the mass flux of solute into or out of the micropores as the time rate of change of average concentration is different in concept than that used to obtain solution.

C_{im} is derived from:

$$C_{im}\ (x,\ t) = \frac{3}{a^3} \int_0^\infty r^2\ C^*\ (x,\ r,\ t)\ dr\ , \tag{55}$$

where C* is the local concentration in the spherical aggregate, r is the radial coordinate and a is the radius of the sphere. The diffusion process out of the spherical particles is described by a similar equation as that in 3.1 i.e.:

$$\frac{\partial C^*}{\partial t} = D^*\ \left(\frac{\partial^2 C^*}{\partial r^2} + \frac{2}{r}\,\frac{\partial C^*}{\partial r}\right)\ . \tag{56}$$

Similar boundary and initial conditions apply, namely:

$$C^*\ (x,\ a,\ t) = C\ (x,\ t) \tag{56a}$$

$$\frac{\partial C^*}{\partial r}\ (x,\ 0,t) = 0\ . \tag{56b}$$

The macropore transport equation is solved for a constant initial concentration (57a) and a semi-infinite profile (57b) as:

$$C\ (x,\ 0) = Cm \tag{57a}$$

$$C\ (\infty,\ t) = 0 \tag{57b}$$

$$C(0,\ t) = Co\ . \qquad (57c)$$

The solution to predict effluent curves from finite systems is given by the flux averaged concentration as follows:

$$C/Cm = (\frac{C}{Cm} - 1)\ \{\frac{1}{2} + \frac{2}{\pi} \int_0^\infty \exp\ (\frac{P}{2} - Zp)\ \sin\ (2\gamma_5\ \lambda^2\ T - Zm)\ \frac{d\lambda}{\lambda}\} + 1 \qquad (58)$$

where $Z_p = \left[\frac{1}{2}\ (r_p + \Omega_1) \right]^{1/2}$, $\qquad Z_m = \left[\frac{1}{2}\ (r_p - \Omega_1) \right]^{1/2}$, $\qquad$ (58a,b)

$$r_p = (\Omega_1^2 + \Omega_2^2)^{1/2}\ , \qquad (58c)$$

$$\Omega_1 = \frac{P^2}{4} + \gamma P\ (1 - \beta)\ R\varphi_1\ ,\ \Omega_2 = 2\gamma P\beta R\lambda^2 + \gamma P\ (1 - \beta) R\varphi_2, \qquad (58d,e)$$

$$\Phi_1 = \frac{3\lambda\ (\sinh 2\lambda + \sin 2\lambda)}{\cosh 2\lambda - \sin 2\lambda} - 3\ , \qquad (58f)$$

$$\Phi_2 = \frac{3\lambda\ (\sinh 2\lambda - \sin 2\lambda)}{\cosh 2\lambda - \cos 2\lambda}\ , \qquad (58g)$$

$$T = \frac{qt}{(\theta + \theta^*)L}\ ,\ \gamma = \frac{D^*\ (\theta + \theta^*)L}{a^2\ q\ R^*}\ ,\quad R = \frac{\theta R + \theta^*\ R^*}{\theta + \theta^*}\ , \qquad (58h,i,j)$$

$$P = vL/D\ \ ,\ \ \beta = \frac{\theta R^*}{\theta R + \theta^*\ R^*}\ \ ,\ \ q = v\theta\ . \qquad (58k,l,m)$$

This solution has been solved numerically by Gauss-quadrature. The computer listing and sample printouts are presented in Appendix B2.

3.3 MODEL 3

In this model no micropore diffusion process is considered in the transport equation. Instead, in considering the conservation of volume the micropore solution is assumed to be included in the initial pore volume. The model is formulated and the solution derived below.

Consider the macropore mass balance equation without micropore diffusion:

$$\frac{\partial}{\partial x} (\theta D \frac{\partial C}{\partial x}) - q \frac{\partial C}{\partial x} = \theta \frac{\partial C}{\partial t} . \tag{59}$$

Significant advantage is gained by recasting this differential equation in a moving coordinate system (Wilson and Gelhar, 1981). The average velocity of macropore liquid is:

$$dx = \frac{q}{\theta} = v \tag{60}$$

or $$\theta dx - q dt = 0 . \tag{61}$$

A function of $\eta(x, t)$ = constant is defined such that

$$\frac{\partial \eta}{\partial x} = \theta \tag{62}$$

and

$$\frac{\partial \eta}{\partial t} = -q . \tag{63}$$

Integrating (62) and then differentiating the result with respect to t and applying conservation of volume of the liquid phase yields:

$$\eta(x, t) = \int_0^x \theta dx - \int_0^t q \, (0, t) \, dt . \tag{64}$$

Using (64), Eq. (59) can now be transformed to the moving coordinate $\eta(x, t)$.

$$\frac{\partial}{\partial \eta} (\theta^2 D \frac{\partial C}{\partial \eta}) = \frac{\partial C}{\partial t} \tag{65}$$

Wilson and Gelhar (1981) assumed that θ and D to be practically constant in the region of rapidly varying concentration and equal to their values at $\eta = 0$.

Eq. (65) can therefore be written as:

$$\frac{\partial^2 C}{\partial \eta^2} = \frac{1}{(\theta^2 D)_{\eta=0}} \frac{\partial C}{\partial t} . \tag{66}$$

By assuming a Green-Ampt front, $(\theta^2 D)_{\eta=0}$ which is normally a function of time, becomes constant. Further, by defining $T = t\theta^2 D$ Eq. (66) becomes:

$$\frac{\partial^2 C}{\partial \eta^2} = \frac{\partial C}{\partial T} . \tag{67}$$

The solution to Eq. (67) subject to the following boundary and initial conditions:

$$C(\infty, t) = C_m , \tag{67a}$$

$$C(-\infty, t) = 0 , \tag{67b}$$

$$C(+\eta, 0) = C_m , \tag{67c}$$

$$C(-\eta, 0) = 0 , \tag{67d}$$

is given by (Nazareth, 1984) as:

$$\frac{C}{C_m} = 1 - \frac{1}{2} \operatorname{erfc} (\eta / \sqrt{4T}) \tag{68}$$

and is valid in the vicinity of $\eta = 0$.

Since a Green-Ampt wetting front has been assumed, Eq. (64) becomes

$$\eta = \theta L - qt \; . \tag{69}$$

Equations (68) and (69) have been evaluated by using a Trapezoidal rule integration. As in the previous solutions, the results of the concentration breakthrough curve have been presented as concentration versus time as well as relative concentration versus pore volumes.

3.4 BREAKTHROUGH CURVES

In this section the solutions developed in Sections 3.1 to 3.3 are used to examine the effects of certain parameters on the shape of the breakthrough curve. Of particular importance are the factors affecting the degree of asymmetry or tailing. For a given column length, the degree of tailing of the breakthrough curve will depend on the size of the aggregate and/or the macro-space liquid velocity (Rao, et al., 1980).

The larger the aggregate size, the longer the diffusion path length and hence the longer the time required for solute concentrations in the micro-space to reach equilibrium with the prevailing concentrations in the macro-space. The time available for transfer of solute from the micro-space to the macro-space is dependent on the liquid velocity in the macro-space. Hence, if the particle size or macro-space liquid velocity are sufficiently large, there will be incomplete mixing of solute between the micro and macro-space solutions, and therefore a tailing effect will be observed in the effluent concentrations. It is obvious that decreasing the aggregate size from one test to another would have similar affects as increasing the diffusion constant in the micro-space, D*. Other factors which influence the shape of the curve are the ratio of micro- to macro-space volume and the length of the column. These parameters are combined in a dimensionless form as:

$$A = \frac{D^*L\theta^*}{a^2 v\theta} .$$

The effects of micro-space diffusion are very pronounced for a value of A = 0.01 in model 1 as shown in curve 1 (Fig. 3.4.1). This corresponds to a relatively large particle radius, a, (keeping all other parameters constant). A smaller particle radius, A = 0.5, yields a more symmetric breakthrough curve (curve 2).

In Fig. 3.4.2, breakthrough curves produced by model 1 and 3 are compared. For a column Peclet number, P of 30, the solutions derived by model 1 with a value of A = 5 (curve 3) closely approximates the solution derived by model 3 (curve 4). Hence, if the radius is sufficiently small or macro-space velocity sufficiently slow, the effects of the micro- to macro-space diffusion can be ignored and model 3 can be used. In this model the micro-space liquid was considered to be part of the initial macro-space liquid. It is important to determine when this solution may be used to predict effluent breakthrough curves, even when the aggragates have a large micro-space volume.

It was noted that, the larger the column Peclet number, the larger the value of A that was required for model 1 to approximate model 3. For instance a column Peclet number of 200 requires A to be 30 for model 1 and 3 to produce similar breakthrough curves.

These observations can be combined with the analysis of Passioura (1971)(refer Section 2.3), to produce the following limiting conditions for predicting breakthrough curves.

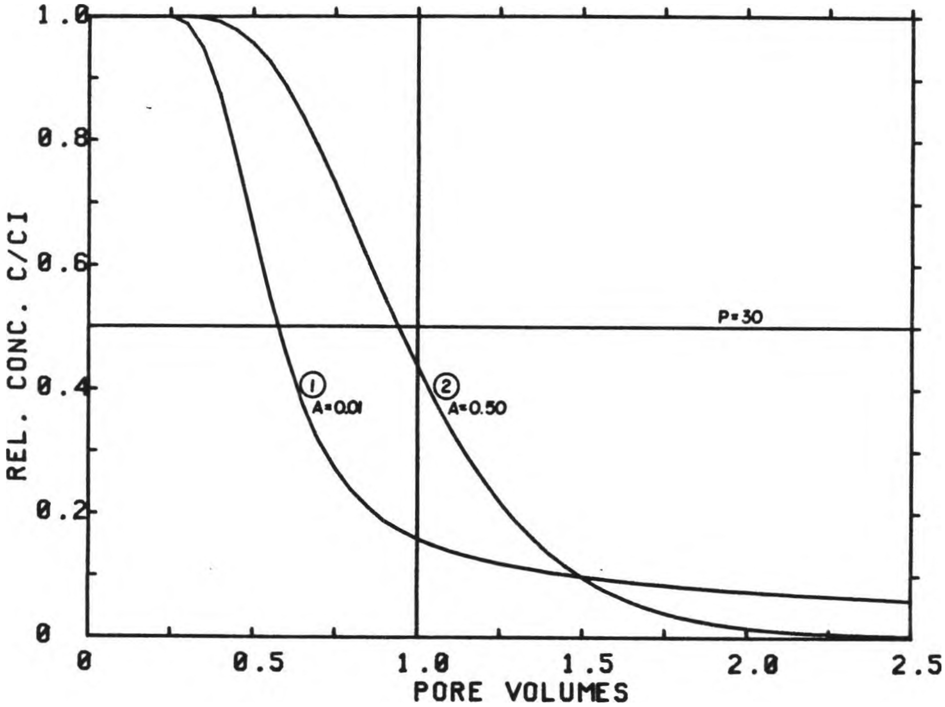

Figure 3.4.1. Breakthrough curves predicted by model 1.

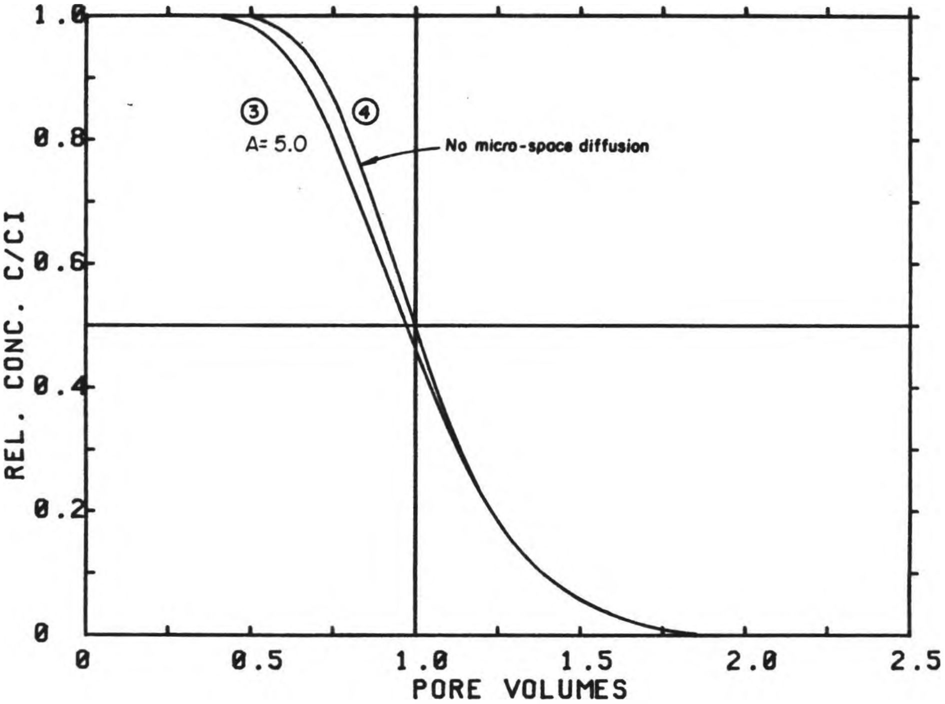

Figure 3.4.2. Comparison of model 1 and model 3 breakthrough curves.

1) For A less than 0.3, the micro- to macro-space diffusion process must be considered as in model 1.

2) For A between 0.3 and approximately 0.16 times the column Peclet number, the macro-space dispersion coefficient can be increased by a factor (Passioura, 1971). A model such as model 3 which does not include the micro-space diffusion process can then be used with an enhanced dispersion coefficient.

3) For A greater than 0.16 times the column Peclet number, model 3 can be used even though the micro-space volume may be relatively large.

The two solutions developed in Sections 3.1 and 3.2 are compared in Figure 3.4.3 for different values of A. For large radii, or small diffusion coefficient, A = 0.01 the solutions are identical; curve 5. For smaller radii, A = 0.50, the two solutions differ slightly as shown in curves 6 and 7. Model 1 predicts higher effluent concentrations for an influent pore volume less than unity. For larger pore volumes model 1 predicts lower effluent concentrations than model 2.

The boundary conditions of these two models are identical and the formulation of the micro- to macro-space diffusion process is essentially the same. In model 1 the source term is considered as the mass flux of solute across the surface area of the spheres, while in model 2 the source term is considered as the rate of change of the average concentration in the spheres. The differences in curves 6 and 7 could therefore only be due to the different methods of analytical solution or the errors in the numerical evaluation of these solutions.

Table 3.1 summarizes the parameters used in the models to produce curves 1 to 7.

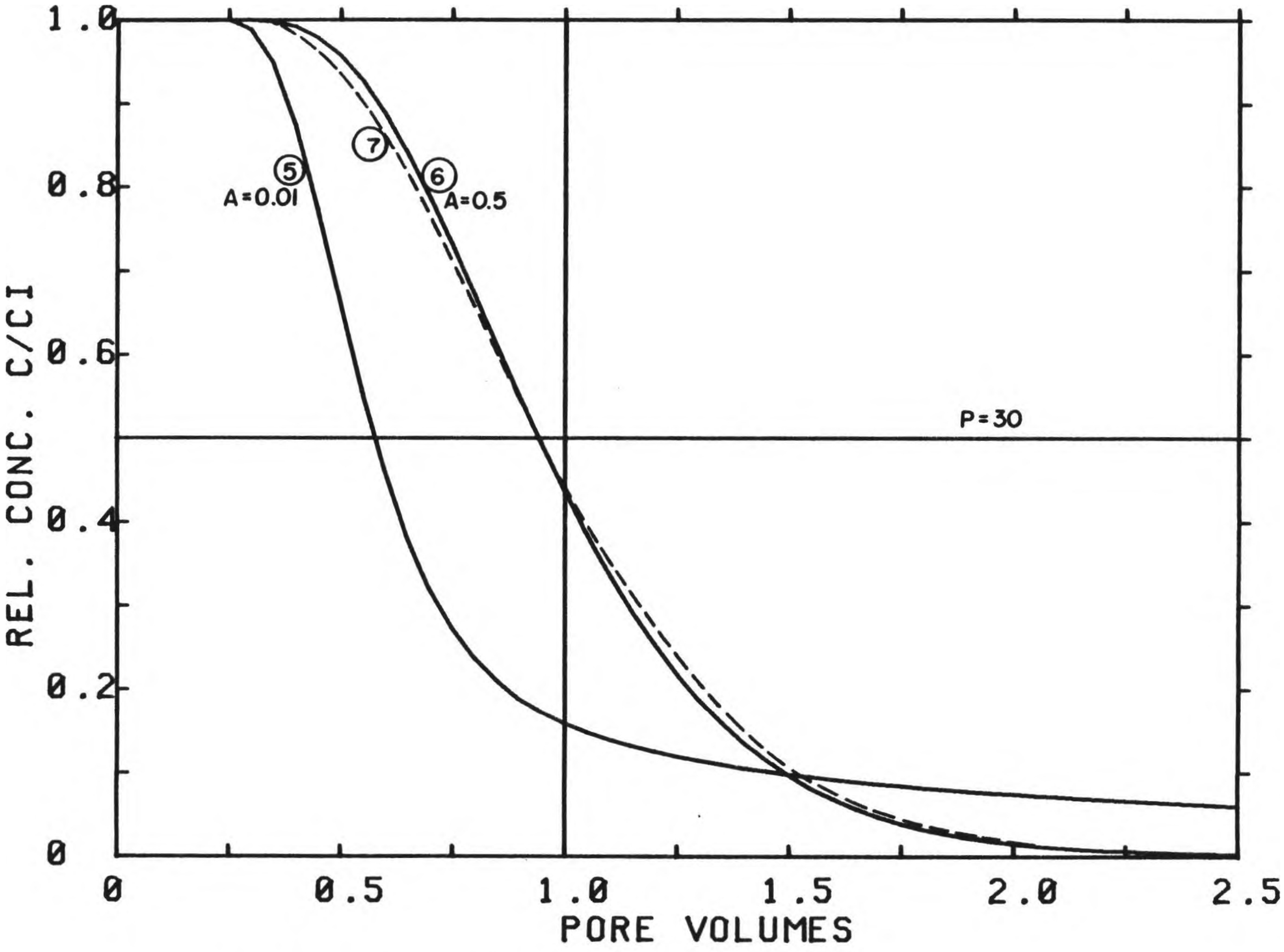

Figure 3.4.3. Comparison of model 1 and model 2.

Table 3.1. Comparison of Solutions

	Model 1					Model 2		Model 3
Parameter	Curve 1	Curve 2	Curve 3	Curve 5	Curve 6	Curve 5	Curve 7	Curve 4
q(cm/hr)	12	12	12	12	12	12	12	12
v(cm/hr)	30	30	30	30	30	30	30	30
L(cm)	30	30	30	30	30	30	30	30
θ	0.4	0.4	0.4	0.4	0.4	0.4	0.4	0.4
θ^*	0.4	0.4	0.4	0.4	0.4	0.4	0.4	0.4
θ_T	0.8	0.8	0.8	0.8	0.8	0.8	0.8	0.4
$D^*(cm^2/hr)$	0.01	0.01	0.01	0.01	0.01	0.01	0.01	---
$D(cm^2/hr)$	30	30	30	30	30	30	30	30
a(cm)	1.0	0.141	0.045	1.0	0.141	1.00	0.141	---
R^*	---	---	---	---	---	1.0	1.0	---
R_m	---	---	---	---	---	1.0	1.0	---
$s(cm^{-1})$	1.2	8.5	26.8	1.2	8.5	---	---	---
A	0.01	0.5	5.0	/01	0.5	0.01	0.5	---
P	30	30	30	30	30	30	30	30
β	---	---	---	---	---	0.5	0.5	---
PV	0 2.5	0 2.5	0 2.5	0 2.5	0 2.5	0 2.5	0 2.5	0 2.5

$$s = \frac{3\theta^*}{a}$$

$$A = \frac{D^* L \theta^*}{a^2 v \theta}$$

$$P = vL/D$$

$$\beta = \frac{\theta R}{\theta R + \theta^* R^*}$$ in Solution 2

$$PV = qt/\theta_T L$$

Chapter 4

LABORATORY PROCEDURES

In this chapter the laboratory procedures used to arrive at an effluent breakthrough curve for a column leach test are described. The models developed in Chapter 3 can only be verified by laboratory test results if each parameter in the model is determined independently from the column leach test. For this reason tests were performed on idealized particles. These particles were spherical in shape and exhibited significant micro-space. All the model parameters could be estimated using test procedures independent of the leach test. The hydrodynamic dispersion coefficients, however, were estimated from test results which are presented in Carbonell et al. (1984). These were then used as a first estimate to fit the analytical solution to the column leach test data. In this way the physical processes upon which the model is based could be verified by the results of the leach tests.

4.1 MATERIAL DESCRIPTION

Three materials were used in a series of column leach tests. Two of these materials comprised nearly spherical particles and hence were considered idealized materials. The results of the leach tests on these two mterials were used to verify the model. The model was then used to predict the shape of the breakthrough curves resulting from leach tests on retorted oil shale material packed to different densities. Unlike the fine grain material used by Nazareth (1984), this oil shale material was coarse grained (Grismer, 1984).

The first idealized material consisted of spherical particles of Aluminum Oxide suitable for chromatographic use. The second material used was one designed as a catalyst carrier for enzyme and microbe immobilization. This material comprises 86% SiO_2 and has a mean intra-particle pore diameter of 8 μm. The retorted oil shale material comprised of varied particle shapes and sizes.

4.2 PHYSICAL PARAMETERS

The tests for estimating the physical parameters required in the model are described here for each material.

4.2.1 Particle size

The particle size distributions of the spherical particles were determined by a sieve analysis for each material. The material was sieved through a range of sieve sizes and the weight of material retained on each sieve was determined. The sieve grading curves for the spherical particles are presented in Figure 4.1. The mean particle diameter for the Al_2O_3 was 0.009 cm. Two sizes of the celite catalyst carrier were used. The mean diameters of these were 0.075 cm and 0.115 cm.

The effective diameter of the oil shales was determined by passing a sample of the material through selected sieve sizes. The value obtained was used as a first estimate in model 1 during curve fitting of the breakthrough curves. It was noted that, for the more densely compacted columns, the average particle size was smaller than for the loosely packed columns. This was due to the particle destruction under

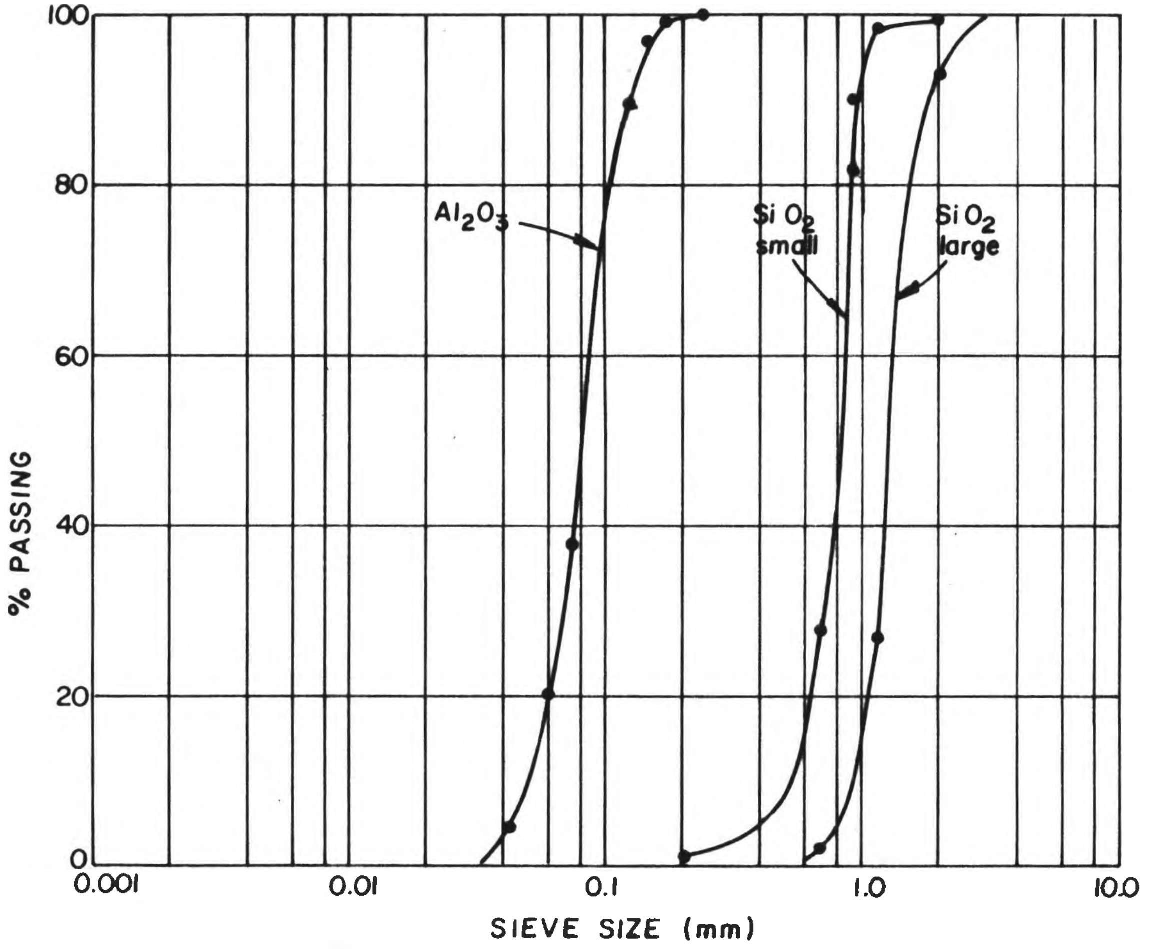

Figure 4.1. Sieve grading curves for spherical particles.

the compactive effort. The mean particle size of these materials before packing was estimated as 1.34 cm.

4.2.2 Micro-space volume

The intra-particle or micro-space volume of the Al_2O_3 particles was estimated by saturating the material and then desaturating a packed sample using a desaturation pressure plate. The residual water content obtained at high pressures was assumed to represent the micro-space volume. The method proceeded as follows:

- A sample of the dry material was placed in a vacuum chamber and a vacuum was applied.
- Water was allowed to enter the chamber under vacuum until the sample was fully submerged. The vacuum was maintained for a minimum of 72 hours to allow for saturation of the micro-space. This procedure was to attempt to remove all air from the micro-space and allow it to fully saturate.
- The water was then drained and the particles packed into small rings 4.92 cm in diameter and 2.56 cm high. The water content at the time of packing was determined on separate samples so that a desired bulk density of the packed material could be achieved.
- The packed rings were then placed in water so that the macro-space would become saturated.
- The samples were placed on the porous plate in a desaturation cell and a pressure was applied.
- The water content of at least two packed samples was determined gravimetrically for each applied pressure ranging from 3.4 kPa to 1550 kPa.

The pressure applied was plotted against degree of saturation. The degree of saturation at which the curve became assymptotic was taken as representing the volume of micro-space. The micro-space volume for the Al_2O_3 particles was estimated as 0.23 cm^3/gm of sample as shown in Figure 4.2.

The micro-space volume of the SiO_2 particles was determined during the process of packing the column. The particles were first saturated under a vacuum and then placed into a suction cup and a suction applied to the ceramic plate. The suction was sufficient to drain water from the macro-space but not sufficient to drain water from the micro-space. When the interparticle solution had been extracted, the particles were removed from the cup and the water content was determined gravimetrically. The average water content was taken to represent the micro-space volume for the test. These ranged from 0.9 cm^3/gm of sample for the smaller particles to 1.4 cm^3/gm of sample for the larger particle size.

Two methods of determining the micro-space of the oil shales were employed using different wetting fluids for each. The first method involved saturating a selected sample of particles with water. The saturation process was allowed to take place under vacuum for at least 24 hours. The particles were then removed from the liquid and placed on a sheet of porous material until the particles appeared dry on the surface. The water content was then determined gravimetrically and taken as representing the volume of water contained in the micro-space.

The second method involved a similar procedure except that after saturation in kerosene, the particles were placed on a suction table. This table comprised of a sheet of porous material hydraulically connected to a reservoir of oil 3 cm below the sheet. Again, the

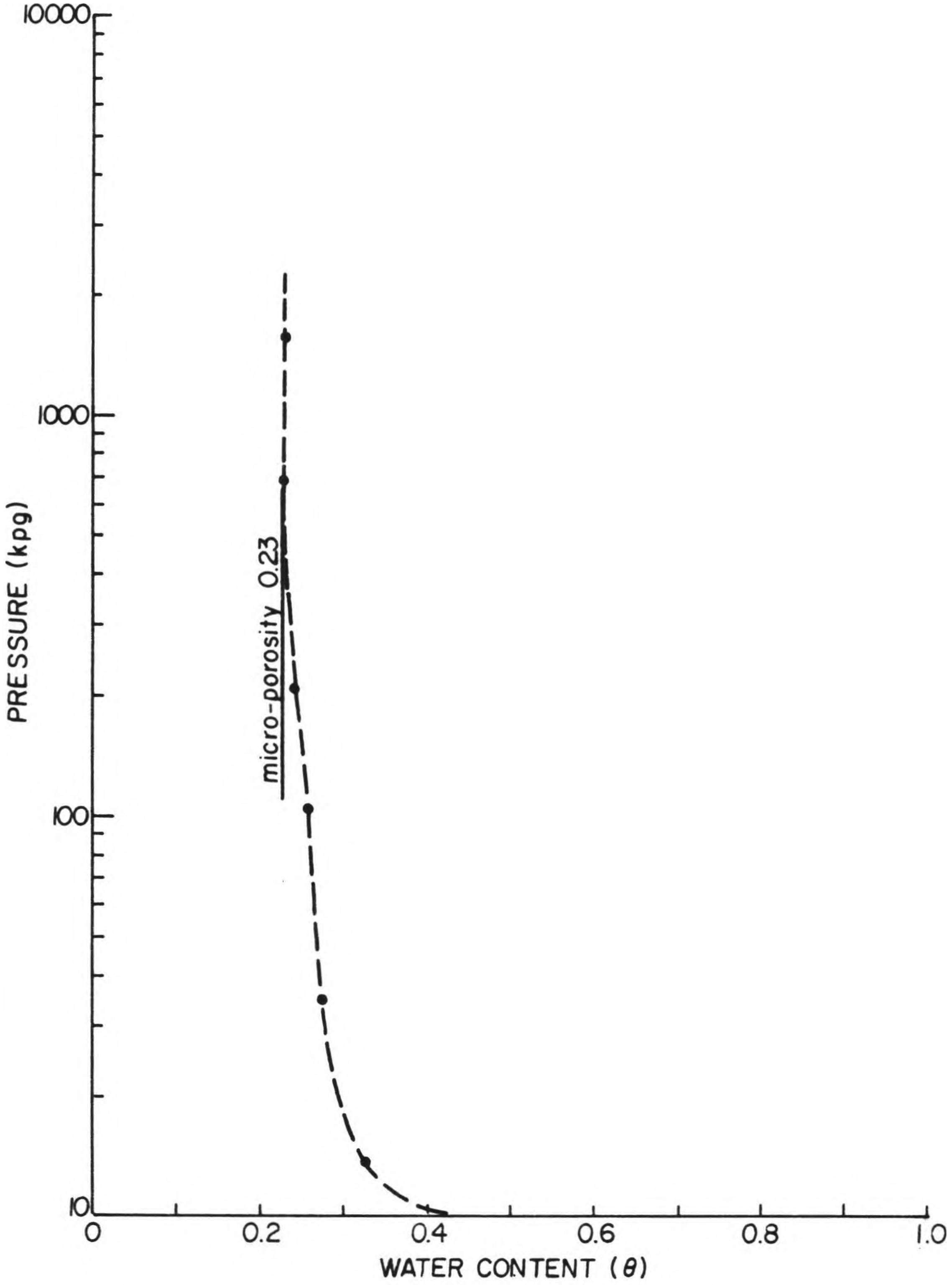

Figure 4.2. Desaturation curve for Al_2O_3 particles.

particles were removed from the sheet when it was assumed that all the liquid had been drawn from their surfaces. This condition was decided by visual inspection of the particles. As in the first method, the liquid content was obtained gravimetrically and assumed to represent the micro-space volume. Table 4.1 summarizes the results for the two methods for different packing densities. The data for these tests are presented in Appendix A1.

Table 4.1. Micro porosity of oil shales.

Packing density (gm/cm^3)	Porosity (cm^3/cm^3)	Microporosity (cm^3/cm^3)	Microporosity (% of total)
	Water Tests		
1.25	0.519	0.235	67.7
1.36	0.477	0.256	53.7
1.52	0.419	0.284	67.7
	Kerosene Tests		
1.25	0.519	0.246	47.4
1.36	0.477	0.268	56.2
1.52	0.419	0.297	70.9

4.2.3 Specific density

The specific densities of the materials were determined gravimetrically by the pycnometer method (ASTM, D854). A 500 ml flask was used instead of the pycnometer. Air was extracted from the water and sample mixture in the flask by applying a vacuum. The test was performed without crushing the particles so that an "effective" solid specific density was obtained. This value could be applied where the micro-space was not effectively filled with water during any of the saturation processes.

The effective specific density obtained for the Al_2O_3 particles was 3.15 gm/cm^3 and that for the SiO_2 particles was 2.31 gm/cm^3. The average specific density obtained for the retorted oil shale was 2.60 gm/cm^3 from the water tests and 2.57 from the kerosene tests. The data for these tests are shown in Appendix A2.

4.3. BATCH DIFFUSION TESTS

A batch diffusion test was used to estimate the intra-particle diffusion coefficients for the spherical particles. The procedure was as follows.

- The particles were saturated under vacuum with a solution of NaCl for at least 24 hours.
- The liquid in the macro-space was then withdrawn from the sample of material. This was done with the desaturation cell for the Al_2O_3 particles and with the suction cup for the SiO_2 particles.
- The samples of the material were placed in a beaker with a specific amount of distilled water. The samples were stirred and the particles allowed to mix freely in the distilled water. The Cl concentration in the macro-space was determined at specific times. This was done for the Al_2O_3 particles by withdrawing a sample of liquid from the beaker at a time of 15 sec. The concentration-time relationship for the SiO_2 particles was determined by measuring the Electrical Conductivity (EC) of the solution

at various time intervals. The EC had been calibrated to yield Cl concentration in the macro-space solution.

The results of these tests are tabulated in Appendix A3 and are summarized in Table 4.2. The diffusion coefficients, D* were estimated by curve fitting as described in Chapter 5.

Table 4.2. Batch Diffusion Test Results

Sample	Time min:sec	Concentration mg/l
1. Al_2O_3	0:15	365
	2:00	359
2. SiO_2 (large)	0:05	103
	0:30	470
	0:40	461
	0:50	555
	1:00	536
	1:15	559
	1:30	555
	1:45	559
	2:00	578
	2:15	611
	3:00	616

4.4 THE COLUMN LEACH TEST

The column leach test performed on the spherical particles in this study was designed to simulate the Equilibrated Soluble Mass or ESM test, Nazareth (1984). In the ESM test chemical equilibrium between the antecedent moisture and the solids is allowed to take place before leaching is initiated.

4.4.1 Material preparation

A sufficient sample of the spherical particles were saturated under vacuum for at least 72 hours to allow the micropores to fill with liquid. The liquid used was a solution of NaCl at a concentration of

800 mg/l for tests on the Al_2O_3 particles and 1600 mg/l for those on the SiO_2 particles.

The sample was then desaturated at a sufficient suction pressure to allow drainage of liquid from the macro-space. On removal from the desaturation cell, the water content of the sample was estimated gravimetrically from small portions of the sample. This water content was recorded and the column packed to the required bulk density. These data, together with the effective particle specific density, permit calculation of the total porosity of the packed material. The macroporosity was determined by subtracting the microporosity from the total porosity.

The oil shale material was prepared somewhat differently. Here the oil shale particles were wetted with a predetermined amount of distilled water, calculated to simulate the field water content. The wetted material was allowed to equilibrate for at least 72 hours before being packed into the columns. The oil shale material was packed at different bulk densities. These were 1.25 gm/cm^3, 1.36 gm/cm^3 and 1.52 gm/cm^3. For the higher bulk densities much compactive effort was required to pack the columns. This resulted in some crushing of the particles and thus the effective sizes determined in 4.2.1 were reduced. This reduction was taken into consideration when calibrating the breakthrough curves.

4.4.2. Test procedure

A schematic diagram of the column is shown in Figure 4.3. The column volume was selected so that the effluent sample volume, which was determined by convenient titration requirements, was only a small fraction of the total pore volume. The average effluent sample was 50 be at least 40 times the mean particle size of the test material (Nazareth, 1984).

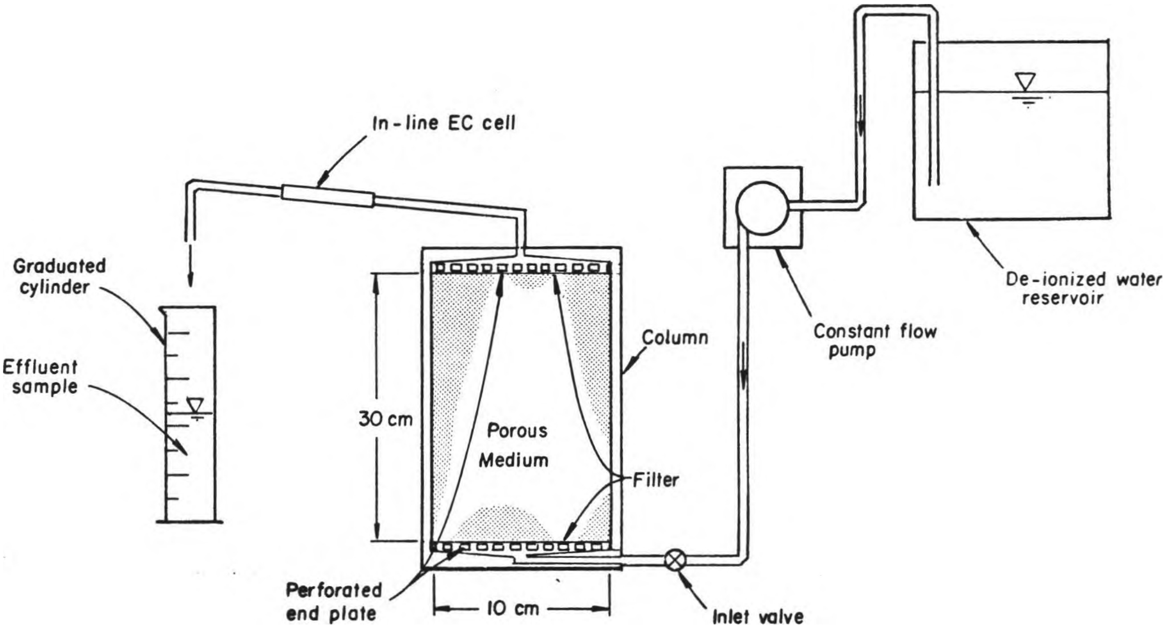

Figure 4.3. Schematic diagram of the column leach test.

The bottom and top end-plates had a 2 mm conical dish machined into the surface. This, together with perforated rigid plates and coarse filters at each end were designed to minimize plate induced tailing effects (Starr and Parlange, 1977).

After packing the column with the prepared material, distilled water was injected at the base. The rate of injection was limited by the requirement that the flow in the porous medium remain in the Darcy flow region. This required that the Reynolds number $R_e = \frac{\rho v d}{\mu}$ be less than 1 (Dybbs et al., 1984). The characteristic length parameter, d is taken as the mean particle diameter while ρ is the fluid density, v the macro-space fluid velocity, and μ, the dynamic viscosity.

The effluent samples were analysed for Cl concentration by titration against $AgNO_3$ using a K_2CrO_4 indicator solution.

A summary of the parameters determined for each column are presented in Table 5.2. The effluent breakthrough data are shown in Appendix A4.

Chapter 5

ANALYSIS AND DISCUSSION

In Chapter 3 it was shown that for very small particles or very low macro-space velocities, the process of diffusion from the micro-space was so rapid that effectively complete mixing of micro and macro space fluids occurred as the macro fluid passed a particle. Therefore, no taling was observed in the breakthrough curve. For relatively large radii or rapid macro-space velocity, however, it was shown that significant asymmetry or tailing of the breakthrough curve resulted. In this chapter the results of column leach tests are used to verify the physical processes modelled.

Three of the parameters used in the model are not derived by direct measurement. These are the effective particle radius, the micro-space diffusion coefficient and the hydrodynamic dispersion coefficient. The estimation of these parameters is described below in Sections 5.1 to 5.3. The results of the effluent breakthrough curves are discussed in Section 5.4.

5.1 EFFECTIVE PARTICLE RADIUS

The solute diffusion out of the spherical aggregates depends on the parameter D^*/a^2 as discussed in Chapter 3. To obtain an effective radius for a material with mixed sizes, a weighted average value of D^*/a^2 is required. Since the volume of micro-space liquid has a significant effect on the process of micro-pore diffusion into the macro-space, it would be advantageous to determine the volume averaged value of D^*/a^2. Rao et al., 1982 suggested the following formula:

$$a = [\sum_{i=1}^{k} (V_i/V_T) a_i^{-2}]^{-1/2}$$

where V_i is the volume of spheres of radius a_i. The sieve analysis curves presented in 4.2.1 where determined on a percentage weight retained basis. These curves were therefore discretized to yield the effective radii of the spherical particles. The following table summarizes the calculations.

Table 5.1. Calculation of effective radius.

Sample	Average radius, a_i (mm)	Fraction of total volume V_i	$V_i a_i^{-2}$	a (mm)
Al_2O_3	0.030 0.0375 0.0425 0.0500	0.2 0.2 0.2 0.2	222 142 110 80	
		1.0	595	0.04
SiO_2 small	0.250 0.350 0.290 0.425 0.475	0.2 0.2 0.2 0.2 0.2	3.2 1.6 1.3 1.1 0.9	
		1.0	8.1	0.35
SiO_2 large	0.425 0.525 0.575 0.600 0.875	0.2 0.2 0.2 0.2 0.2	1.10 0.73 0.60 0.56 0.26	
		1.0	3.25	0.55

The effective radii are therefore

Al_2O_3 $a = 0.004$ cm

SiO_2 small $a = 0.035$ cm

SiO_2 large $a = 0.055$ cm .

5.2 MICRO-SPACE DIFFUSION COEFFICIENT

The diffusion coefficients were determined by curve fitting the results of the batch tests described in 4.3. The solution used to curve fit the data was that for diffusion out of spherical particles into a surrounding liquid of varying concentration. The applicable differential equation, initial and boundary conditions are:

$$\frac{\partial C^*}{\partial t} = D^*\left[\frac{\partial^2 C^*}{\partial r^2} + \frac{2\partial C^*}{r\,\partial r}\right] \tag{5.1}$$

$$C^*(r,o) = C^*_m \tag{5.1a}$$

$$C^*(a,t) = C(t) \tag{5.1b}$$

$$C(0) = 0 \tag{5.1c}$$

where $C^*(r,t)$ is the concentration in the spheres.

$C(t)$ is the concentration in the macro-space liquid and is given by

$$C(t) = \frac{\theta^*}{\theta}(C^*_m - \bar{C}^*\,(t)) \tag{5.2}$$

where θ^* and θ are the volumetric liquid contents in the micro- and macro-space respectively

The average concentration in the spheres at time, t is

$$\bar{C}^* (t) = \frac{3}{a^3} \int_0^a r^2 \, C^*(r,t)dr \qquad (5.3)$$

Equations 5.1 and 5.3 have been solved in Crank, 1975 to yield:

$$\bar{C}^* (t) = C^\infty - (C^*_m - C^\infty) \sum_{n=1}^{\infty} [\frac{6\beta(\beta+1)}{9+9\beta+q_n^2\beta^2}] \exp[\frac{-D^* q_n^2 t}{a^2}] \qquad (5.4)$$

where $C^\infty = \frac{\text{mass of initial solute}}{\text{total volume of liquid}} = \frac{\theta^* C^*_m}{\theta + \theta^*}$

$\beta = \frac{\theta}{\theta^*}$

and q_n are the roots of $\tan (q_n) = (\frac{3q_n}{3 + \beta q_n^2})$

Combining 5.2 and 5.4 yields

$$C(t) = \frac{1}{\beta} (C^*_m - C^\infty) \left| \left(1 - \sum_{n=1}^{\infty} [\frac{6\beta(\beta + 1)}{9 + 9\beta + + q_n^2\beta^2}] \exp [\frac{-D^* q_n^2 t}{a^2}] \right) \right|$$

This solution was fitted to the data for the batch diffusion tests as shown in Figure 5.1.

A value of $D^* = 0.012$ cm^2/hr provided a good fit for both the Al_2O_3 and the SiO_2 particles, although only one data point was obtained for the Al_2O_3 particles. The molecular diffusion coefficient for NaCl in an aqueous solution, $D_o = 0.054$ cm^2/hr was extracted from the CRC Handbook for Chemical Engineers, 64th Ed. Dividing this value by D^* yields the tortuosity of the micro-space, $\tau^2 = 4.5$. The value of D^* was also determined by Rao et al. (1980a) for the diffusion of ^{36}Cl out of ceramic spheres. This value was therefore used in curve fitting the breakthrough data for the spherical particles as well as the oil shale material.

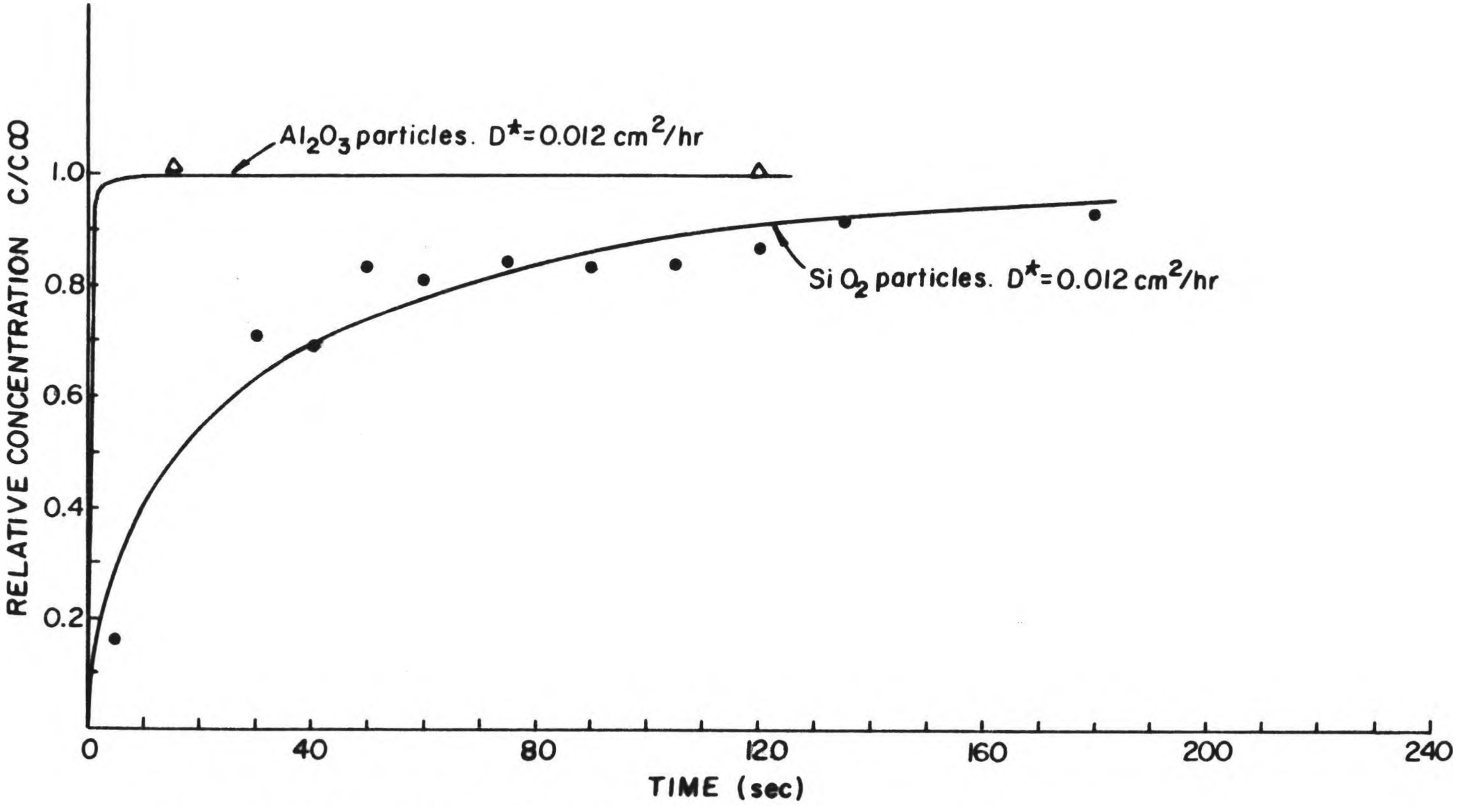

Figure 5.1. Batch diffusion test.

5.3 HYDRODYNAMIC DISPERSION COEFFICIENT

A first estimate of the dispersion coefficient was abstracted from Carbonell and Whitaker, 1984. These authors present curves of experimental values of D/D_o versus the particle Peclet number. Here D is the dispersion coefficient and D_o the molecular diffusion coefficient. The particle Peclet number, Pe_p is determined from:

$$Pe_p = \frac{vd}{D_o} \left(\frac{\phi}{1 - \phi} \right)$$

where d is the average particle diameter, ϕ is the macroporosity and v is the fluid velocity in the macro-space. The values of D determined from these curves are shown in Table 5.2. The hydrodynamic dispersion coefficient was the only parameter varied in curve fitting the breakthrough curve data.

5.4 BREAKTHROUGH CURVES

The experimental data and fitted breakthrough curves (BTC) are shown in Figures 5.2 to 5.5. The BTC for the Al_2O_3 particles is practically symmetrical (Figure 5.2) and could be closely predicted by model 3 even though the micro-space porosity is relatively large (23 percent by volume). The value of the dimensionless parameter, A for this case was 1045, which indicates that the micro-space diffusion process can be neglected. For an increased particle size and Darcy velocity, the asymmetry and the tailing effect of the BTC become more pronounced. This can be seen in the curves for the larger SiO_2 particles. The BTC in Figure 5.3 is for the smaller of the SiO_2 particles. Here the parameter A is 0.29 and thus, according to the limitations set out in Chapter 3, a model which takes into account the micro-space diffusion process must be used. Model 1 was able to predict the experimental BTC. The fitted value for the dispersion coefficient, 90 cm^2/hr was close to that extracted from the literature, 80 cm^2/hr.

Figure 5.4 compares two BTCs for the larger of the SiO_2 particles. The only parameter varied from the one test to the other was the macro-space velocity. It can be seen that for the lower velocity, A = 2.1, the BTC is nearly symmetrical whereas for the larger velocity, A = 0.43 there is some tailing to the BTC. Both sets of BTC data are fitted using model 1. The values of the dispersion coefficients were close to those extracted from the literature (refer Table 5.2).

The BTCs for the oil shale material are shown in Figure 5.5. Model 1 predicted the BTC for the densely packed material which had a relatively small radius and parameter A = 0.59. For the loosely packed material with large mean radius, A = 0.04 model 1 failed to predict the lower end of the curve accurately although the data and model show significant tailing of the BTC. The lack of fit between model and experimental data for this case could be due to the nonspherical shape of the particles.

The values of the hydrodynamic dispersion coefficient determined by fitting the model to the data compare favorably with those extracted from the literature for the tests on the SiO_2 particles. However, these values do not compare well for the tests on the Al_2O_3 particles and the oil shale particles. This could be due to the fact that the Green-Ampt wetting front assumption is a good approximation for the flow in the relatively large SiO_2 particles and less so for the Al_2O_3 particles. The hydrodynamic dispersion coefficient determined by tests on saturated spherical particles would then be applicable. However, for the relatively small Al_2O_3 particles, a more complex mechanism of

Table 5.2. Model 1 parameters.

Test #	Material	Column Length cm	Average Radius cm	Average Pore Vel. cm/hr	θ (sat)	θ*	D* cm^2/hr	D (fitted) cm^2/hr	D (first estimate) cm^2/hr **
1	Al_2O_3	30	0.004	11.04	0.450	0.230	0.012	1.35	0.04
2	SiO_2	16	0.035	357	0.450	0.294	0.012	90	80
3		30	0.055	262	0.449	0.426	0.012	60	90
4		30	0.055	48	0.468	0.401	0.012	20	15
5	***Oil Shale	91	1.75	7.64	0.279	0.241	0.012	5	30
6		91	0.50	16.69	0.129	0.291	0.012	10	5

**Extracted from Carbonell et al. (1984).
***Grismer (1984).

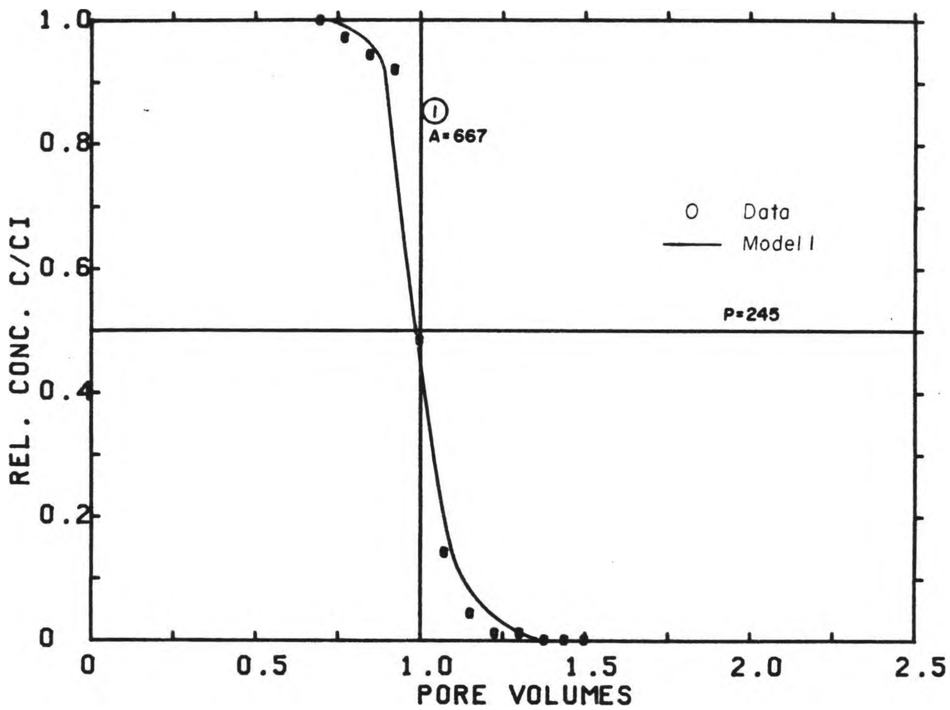

Figure 5.2. Breakthrough curve for spherical Al_2O_3 particles (a = 0.005 cm).

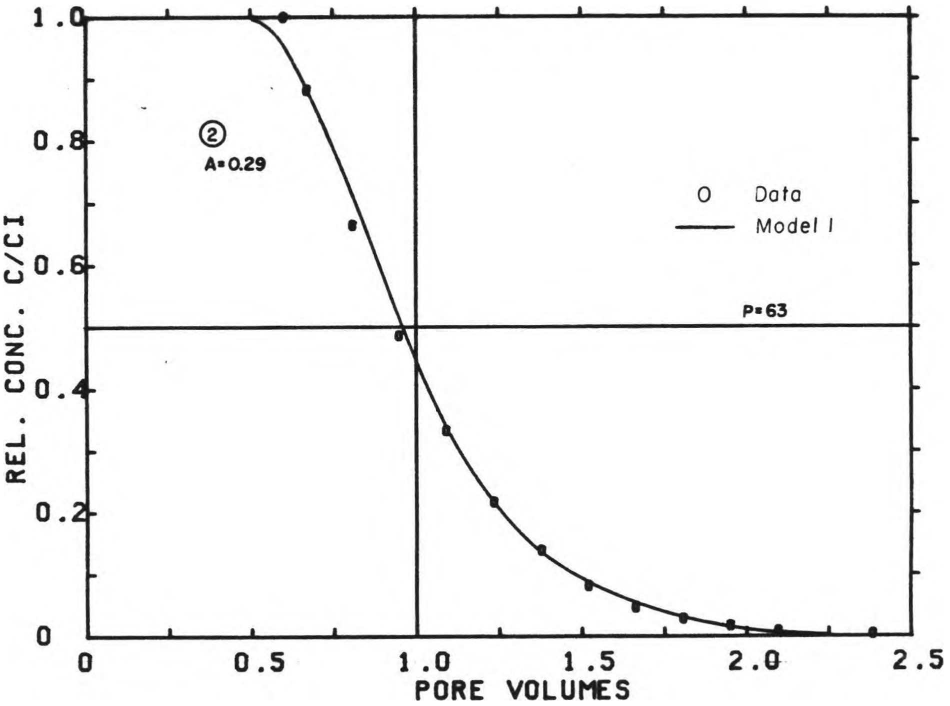

Figure 5.3. Breakthrough curve for spherical SiO_2 particles (a = 0.035 cm).

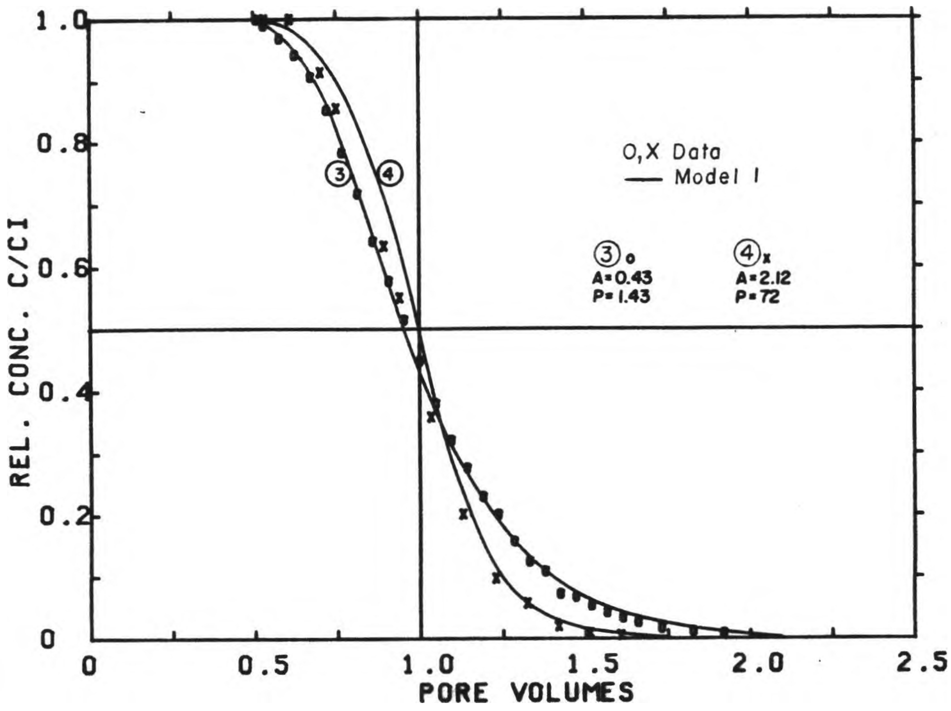

Figure 5.4. Breakthrough curves for spherical SiO_2 particles (a = 0.055 cm).

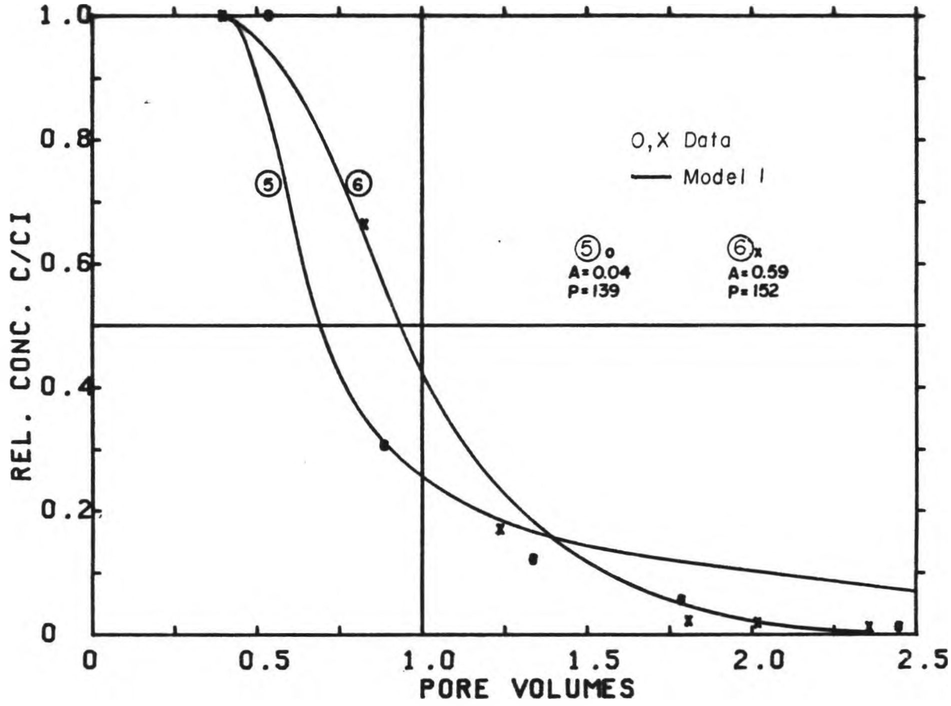

Figure 5.5. Breakthrough curve for retorted oil shale (Grismer, 1984).

unsaturated flow may occur and hence a dispersion coefficient determined from tests on saturated materials would not be applicable. A similar argument is applicable for the oil shale material which has a significant percentage of fines and clayey material. Hence a Green-Ampt model for the unsaturated flow in this material may also be inaccurate.

These observations concur with the findings of Nazareth (1984) who showed that dispersion for a Green-Ampt case would be expected to be different from a truly unsaturated case. Thus the "effective" dispersion coefficient depends upon whether the flow was saturated or not. Awad (1986) concluded from tests on sand materials that the hydrodnamic dispersion coefficient increases with increasing seepage velocity and decreasing volumetric solution content. Examination of Table 5.2 reveals this to be true for the Al_2O_3 material and the densely packed oil shale column. These two tests were the most likely to have truly unsaturated flow and hence the least likely to have a Green-Ampt type wetting front. An increased dispersion coefficient would therefore be expected.

Chapter 6

CONCLUSIONS AND RECOMMENDATIONS

The physical process of diffusion from an immobile phase into a mobile phase during solute transport in porous media has been analyzed. An analytical model which includes this process has been developed. The combination of physical parameters which determine the significance of this process has been studied. The following conclusions are drawn.

- The parameter $A = \frac{D^*L\theta^*}{a^2 v\theta}$ can be used to determine when a model which includes the micro-space diffusion mechanism must be used to predict effluent breakthrough curves. The effects of this mechanism must be considered when A is less than 0.3.
- For a value of A greater than 0.16 times the column Peclet number, the diffusion process may be neglected even though the material may exhibit a significant micro-space volume. In this case the immobile phase may be assummed to exist initially within the macro-space and a simple solute transport model used.
- The model which includes the diffusion process was able to predict effluent breakthrough curves of materials in which a Green-Ampt type unsaturated flow process was applicable. In this case all the model parameters were derived independently from the column leach test. Values of hydrodynamic dispersion for saturated flow were taken from the literature and used as a first estimate in the model. The final values compared well with these first estimates.

- For materials in which the Green-Ampt assumption was not valid, the breakthrough curve data could be fitted with the model by calibrating the hydrodynamic dispersion coefficient. In these cases the final value of the hydrodynamic dispersion coefficient was greater than that taken for saturated flow.

From the results of this study the following recommendations are made:

- The model which includes the diffusion process could be developed further to include an unsaturated flow process where the water content varies in time and space. Alternatively, experimental tests could be performed to determine an effective value of hydrodynamic dispersion for cases where the Green-Ampt model is not valid.
- Tests should be performed on materials which have larger particles than those used in this study and a greater mix of particle sizes in order to verify the model for values of $A<<0.3$.

REFERENCES AND BIBLIOGRAPHY

Aifantis, E. C., On Barenblatt's Problem, International Journal of Engineering Science, Vol. 18, No. 6.

Aifantis, E. C. and Hill, J. M., 1980. On the Theory of Diffusion in Media with Double Diffusity I. Basic Mathematical Results. Q. J. Mech. Appl. Math., Vol. XXXIII, Pt. I.

Awad, M. M., 1986. Effect of Solution Content and Seepage Velocity on Hydrodynamic Dispersion. Ph.D. Dissertation, Colorado State University.

Baker, L. E., 1977. Effects of Dispersion and Dead-end Pore Volume in Miscible Flooding. Society of Petroleum Engineers Journal, June.

Baker, J. A. and Foster, S. D., 1981. A Diffusion Exchange Model for Solute Movement in Fissured Porous Rock. Q. J. Eng. Geol. London, Vol. 14.

Bear, J. and Corapcioglu, M. Y., 1984. Fundamentals of Transport Phenomena in Porous Media. Nato ASI Series E, No. 82, Martinus Nijhoff Publ..

Bryant, M. A., 1982. Dispersion in Bimodal Oil Shales. M. S. Thesis, CSU.

Cameron, D. R. and Klute, A., 1977. Convective Dispersive Solute Transport with a Combined Equilibrium and Kinetic Adsorption Model. Water Resources Res., 13.

Carbonell R.G. and Whitaker, S., 1984. Heat and Mass Transfer in Porous Media. In: Fundamentals of Transort Phenomena in Porous Media, Ed. Bear, J. and Yavuz Corapcioglu, M. NATO ASI Series E. Applied Sciences 82. Martinus Nijhoff Publishers.

Coats, K. H. and Smith, B. D., 1964. Dead-end Pore Volume and Dispersion in Porous Media. Society of Petroleum Engineers Journal, March.

Corey, A. T., 1977. Mechanics of Heterogenous Fluids in Porous Media. Water Resources Publications.

De Smedt, F. and Wierenga, P. J., 1979. A Generalized Solution for Solute Flow in Soils with Mobile and Immobile Water. Water Resources Research, Vol. 15, No. 5, October.

Dybbs, A and Edwards, R.V., 1984. A New Look at Porous Media Fluid Mechanics - Darcy to Turbulent. In: Fundamentals of Transort Phenomena in Porous Media, Ed. Bear, J. and Yavuz Corapcioglu, M. NATO ASI Series E. Applied Sciences 82. Martinus Nijhoff Publishers.

Freeze, R. H. and Cherry, J. A., 1979. Groundwater. Prentice-Hall, Inc., New Jersey.

Gaudet, J. P., Jegat, H., Vachaud, G. and Wierenga, P. J., 1977. Solute Transfer with Exchange Between Mobile and Stagnant Water Through Unsaturated Sand. Soil Science Society of America Journal, Vol. 41, No. 4, Jul/Aug.

Goodknight, R. C., Klikoff Jr., W. A. and Fatt, I., 1970. Non-Steady-State Fluid Flow and Diffusion in Porous Media Containing Dd-end Pore Volume. Soil Science Society of America Journal, Vol. 40.

Grisak, G. E., Pickens, J. F. and Cherry, J. A., 1980. Solute Transport Through Fractured Media 2. Column Study of Fractured Till.

Grisak, G. E. and Pickens, J. F., 1980. Solute Transport Through Fractured Media 1. The Effect of Matrix Diffusion. Water Resources Research, Vol. 16, No. 4.

Grismer, M., 1984. Notes on Laboratory Leaching and Permeability Tests on Oil Shales. Unpublished notes.

Hill, J. M. and Aifantis, E. C., 1980. On the Theory of Diffusion in Media with Double Diffusivity, 11. Boundary Value Problems. Q. J. Mech. Appl. Math., Vol. 33, Pt. 1.

Hill, D. E. and Parlange, J. Y., 1980. Wetting Front Instibility in Layered Soils. Soil Science Soc. of Am. Proc. 36.

Kasten, P. R., Lapidus, L. and Admunson, N. R., 1952. Mathematics of Adsorption in Beds. V. Effect of Intraparticle Diffusion in Flow Systems in Fixed Beds. Journal of Physical Chemistry, Vol. 56.

Lai and Jurinack, 1971. Numerical Approximation of Cation Exchange in Miscible Displacement Through Soil Columns. Soil Sci. Soc. of Am. Proc. 35.6.

Lapidus, L. and Admunson, N. R., 1952. Mathematics of Adsorption in Beds, VI. The Effect of Longitudinal Diffusion in on Exchange and Chromatographic Columns. Journal of Physical Science, Vol. 56, Nov. 1952.

Laryea, K. B., Elrick, D. E. and Robin, M. J. L., 1982. Hydrodynamic Dispersion Involving Cationic Adsorption During Unsaturated, Transient Water Flow in Soil. Soil Science Soc. of Am. Journal, Vol. 46, No. 4, Jul/Aug.

Lindstrom, F. T. and Boersma L., 1973. A Theory on the Mass Transport of Previously Distributed Chemicals in A Water-Saturated Sorbing Porous Medium: III. Exact Solution for First-Order Kinetic Sorbtion. Soil Science, Vol. 115, No. 1.

Lindstrom, F. T. and Narasimham, M. N. L., 1973. Mathematical Theory of a Kinetic Model for Dispersion of Previously Distributed Chemicals in a Sorbing Porous Medium. SIAM Journal Applied Mathematics, Vol. 24, No. 4.

Nazareth, V. A., 1984. A Laboratory Leach Test for Oil Shale Solid Wastes. Ph.D. Dissertation, Colorado State University.

Nielsen, D. R. and Biggar, J. W., 1961. Miscible Displacement in Soils: I. Experimental Information. Soil Science Society of America Proceedings, Vol. 25, No. 1.

Nkedi-Kizza, P., 1979. Ion Exchange in Aggregated Porous Media During Miscible Displacement. Ph.D. Dissertation. Univ. of California, Davis.

Nkedi-Kizza, P., Biggar, J. W., Van Genuchten, M. T., Wierenga, P. J., Selim, H. M., Davidson, J. M. and Nielsen, D. R., 1983. Modelling Tritium and Chloride 36 Transport Through an Aggregated Oxisol. Water Resources Research, Vol. 19, No. 3, June.

Parker, J. C. and Van Genuchten, M. T., 1984. Flux-Averaged and Volume-Averaged Concentrations in Continuum Approach to Solute Transport. Water Resources Research, Vol. 20, No. 7, July.

Parlange, J. Y., Starr, J. L., Barry, D. A. and Braddock, R. D., 1982. Theoretical Study of the Inclusion of Dispersion in Boundary Conditions and Transport Equations for Zero-order Kinetics. Soil Science Soc. of Am. Journal, Vol. 46.

Passioura, J. B., 1971. Hydrodynamic Dispersion in Aggregated Media, 1. Theory 11. Effects of Velocity in Aggregate Size. Soil Sci. 111.

Perkins, T. K. and Johnston, O. C., 1963. A Review of Diffusion and Dispersion in Porous Media. Society of Petroleium Engineers Journal, March.

Philip, J. R., 1968. Diffusion, Dead-end Pores and Linearized Adsorption in Aggregated Media. Aust. J. Soil Res., Vol. 6.

Pinner, A. and Nye, P. H., 1982. A Pulse Method for Studying Effects of Dead-end Pores, Slow Equilibration and Soil Structure on Diffusion of Solutes in Soil. Journal of Soil Science, Vol. 33.

Roa, P. S., Davidson, J. M., Jessup, R. E. and Selim, H. M., 1979. Evaluation of Conceptual Models for Describing Nonequilibrium Adsorbtion-Desorption of Pesticides During Steady Flow in Soils. Soil Science Society of America Journal, Vol. 43.

Roa, P. S., Jessup, R. E. and Addiscott, T. M., 1982. Experimental and Theoretical Aspects of Solute Diffusion in Spherical and Nonspherical Aggregates. Soil Science, Vol. 133, No. 6, June.

Roa, P. S., Jessup, R. E., Rolston, D. E., Davidson, J. M. and Kilcrease, D. P., 1980a. Experimental and Mathematical Description of Nonadsorbed Solute Transfer by Diffusion in Spherical Aggregates. Soil Science Society of America, Vol. 44.

Roa, P. S., Rolston, D. E., Jessup, R. E. and Davidson, J. M., 1980b. Solute Transport in Agregated Porous Media: Theoretical and Experimental Evalution. Soil Science Society of America, Vol. 44.

Rasmuson, A. and Neretnieks, I., 1980. Exact Solution of a Model for Diffusion in Particles and Longitudinal Dispersion in Packed Beds. AIChE Journal, Vol. 26, No. 4., July.

Saxena. Effects of Pore Size on Diffusion Coefficient in Porous Media. Soil Science, 117.

Skopp, J. and Warrick, A. W., 1974. Two-Phase Model for the Miscible Displacement of Reactive Solutes in Soils. Soil Science Society of America Vol. 38, No. 4, Jul/Aug.

Starr, J. L. and Parlange, J. Y., 1977. Plate-Induced Tailing in Miscible Displacement Experiments. Soil Science, Vol. 124, No. 1.

Starr, J. L. and Parlange, J. Y., 1979. Dispersion in Soil Columns: The snow Plow Effect. Soil Science Society of America Journal, Vol. 43.

Sudicky, E. A. and Frind, E. O., 1982. Contaminant Transport in Fractured Porous Media: Analytical Solutions for a System of Parallel Fractures. Water Resources Research, Vol. 18, No. 6, Dec.

Tang, D. H., Frind, E. O. and Sudicky, E. A., 1981. Contaminant Transport in Fractured Porous Media: Analytical Solution for a Single Fracture. Water Resources Research, Vol. 17, No. 3, June.

Van Genuchten, M. T., 1981. Nonequilibrium Transport Parameters from Miscible Displacement Experiments. USDA Science and Education Admin. U.S. Salinity Lab Research Report, No. 119.

Van Genuchten, M. T., 1985. A General Approach for Modeling Solute Transport in Structured Soils. Proc. 17th Int. Congress, Int. Assoc. of Hydrogeologists "Hydrogeology of Rocks of Low Permeability", Jan.

Van Genuchten, M. T. and Alves, W. J., 1982. Analytical Solutions of the One-Dimensional Convective-Dispersive Solute Transport Equation. USDA Technical Bulletin, No. 1661.

Van Genuchten, M. T. and Wierenga, P. J., 1976. Mass Transfer Studies in Sorbing Porous Media I. Analytical Solutions. Soil Science Society of America Journal, Vol. 40, No. 4, Jul/Aug.

Wilson, J. L. and Gelhar, L. W., 1981. Analysis of Longitudinal Dispersion in Unsaturated Flow. Water Resources Research, Vol. 17, No. 1, Feb.

APPENDIX A1

MICRO-POROSITY TEST RESULTS

A1.1. Al_2O_3 desaturation curve.

Sample	Density of Packed Ring ρ_b	Total Porosity ϕ_T	Water Content by Mass w	Water Content by Volume θ	Degree of Saturation $S = \theta/\phi_T$	Pressure
	(gm/cm)	(cm^3/cm^3)	(gm/gm)	(cm^3/cm^3)		(psi)
1	1.577	0.692	0.580	0.572	0.826	0.5
2	1.569	0.694	0.593	0.581	0.837	0.5
3	1.555	0.697	0.590	0.571	0.820	0.5
4	1.591	0.690	0.573	0.563	0.816	1.0
5	1.551	0.697	0.567	0.544	0.780	1.0
6	1.553	0.697	0.568	0.539	0.773	1.0
7	1.592	0.690	0.336	0.336	0.487	2.0
8	1.598	0.689	0.330	0.326	0.473	2.0
9	1.550	0.698	0.281	0.271	0.388	5.0
10	1.553	0.698	0.281	0.270	0.387	5.0
11	1.551	0.698	0.281	0.273	0.391	5.0
12	1.515	0.689	0.250	0.251	0.364	14.8
13	1.484	0.695	0.251	0.248	0.357	14.8
14	1.524	0.687	0.252	0.258	0.376	14.8
15	1.503	0.691	0.244	0.243	0.352	30.0
16	1.508	0.690	0.243	0.243	0.352	30.0
17	1.494	0.693	0.247	0.243	0.351	30.0
18	1.622	0.687	0.222	0.223	0.325	100
19	1.585	0.694	0.222	0.215	0.310	100
20	1.593	0.692	0.222	0.215	0.311	100
21	1.611	0.681	0.230	0.236	0.347	225
22	1.572	0.688	0.229	0.228	0.331	225
23	1.620	0.679	0.229	0.229	0.337	225

A1.2. SiO_2 microporosity.

Sample	Wet Mass (gm)	Dry Mass (gm)	Water Content (gm/gm)	Bulk Density (gm/cm^3)	Microporosity (cm^3/cm^3)
Column 1	300.22	158.43	0.895	0.328	0.294
Column 2	1735.49	699.47	1.481	0.288	0.426
Column 3	1711.90	735.04	1.329	0.302	0.401

A1.3. Oil shale microporosity (using water).

Particle Size (mm)	Wet Mass (gm)	Dry Mass (gm)	Volume of Water in Micropores (cm^3)	Microporosity (cm^3/gm)
>19.1	57.45	48.52	8.95	18.4
13.33-19.1	183.04	156.14	26.96	17.3
9.423-13.33	168.84	141.10	27.80	19.7
6.680-9.423	154.99	128.79	26.26	20.4
3.926-6.680	122.45	103.83	18.66	18.0
			Average	18.8

A1.4. Oil shale microporosity (using kerosene).

Particle Size (mm)	Wet Mass (gm)	Dry Mass (gm)	Volume of Kerosene in Micropores (cm^3)	Microporosity (cm^3/gm)
>19.1	55.69	48.58	8.80	18.1
13.33-19.1	158.66	138.82	24.56	17.7
9.423-13.33	160.61	138.40	27.49	19.9
6.680-9.423	152.56	128.88	29.31	22.7
3.926-6.680	91.57	78.71	15.92	20.2
				19.7

APPENDIX A2

PARTICLE SPECIFIC GRAVITY TEST RESULTS

A2.1. Al_2O_3 specific gravity.

Sample	Mass of Flask (gm)	Mass of Flask + Water (gm)	Water Temp. °C	Mass of Flask + Water + Solid (gm)	Dry Mass of Solid (gm)	Specific Density (gm/cm^3)
1	31.37	61.59	21.5	65.33	5.46	3.174
2	33.66	62.44	21.5	65.83	4.93	3.204
3	31.43	61.62	21.5	71.17	14.23	3.041
4	33.72	62.49	21.5	71.78	13.64	3.136
5	152.25	640.57	21.5	684.66	63.98	3.122
6	183.96	682.22	22.0	745.70	91.71	3.249
					Average	3.15

A2.2. SiO_2 specific gravity.

Sample	Mass of Flask (gm)	Mass of Flask + Water (gm)	Water Temp. °C	Mass of Flask + Water + Solid (gm)	Dry Mass of Solid (gm)	Specific Density (gm/cm^3)
1	103.30	352.57	22	360.57	13.99	2.336
2	105.07	354.40	22	362.50	14.40	2.286
3	183.63	681.66	22	703.79	183.63	2.317
4	178.84	676.87	22	709.15	178.84	2.300
					Average	2.31

A2.3. Oil shale specific gravity (by water).

Particle Size (mm)	Mass of Flask (gm)	Mass of Flask + Water (gm)	Water Temp (°C)	Mass of Flask + Water + Solid (gm)	Dry Mass of Solids (gm)	Specific Gravity of Solid (gm/cm^3)
>19.1	81.67	313.31	22	344.887	50.12	2.70
13.33-19.1	81.81	313.53	22	411.07	157.54	2.63
9.423-13.33	99.02	321.10	22	408.74	142.64	2.59
6.680-9.423	81.68	313.30	22	392.65	130.14	2.56
3.926-6.680	98.88	321.55	22	384.12	103.78	2.52
					Average	2.60

A2.4. Oil shale specific gravity (by kerosene).

Particle Size (mm)	Mass of Pycnometer (gm)	Mass of Pycnometer + Kerosene (gm)	Temp (°C)	Mass of Pycnometer + Kerosene + Solid (gm)	Dry Mass of Solids (gm)	Specific Gravity of Solid (gm/cm^3)
13.33-1.1	33.69	57.01	22	70.79	20.09	2.57
9.423-13.33	31.38	55.7	22	68.51	18.53	2.54
6.680-9.423	33.6	57.01	22	69.04	17.37	2.63
3.926-6.680	31.38	55.91	22	67.39	16.84	2.54
					Average	2.57

APPENDIX A3

BATCH DIFFUSION TEST RESULTS

A3.1. Al_2O_3 batch diffusion.

Sample	Wet Mass of Sample (gm)	Volume of Water Added (ml)	Time Extracted min:sec	Concentration [NaCl] mg/l	Relative Concentration C/C_∞
1	25	50	0:15	365	1.01
2	25	50	2:00	359	1.00

A3.2. SiO_2 batch diffusion.

Sample	Wet Mass of Sample (gm)	Dry Mass of Sample (g)	Volume of Water Added (ml)	Time of Reading min:sec	Concentration [NaCl] (mg/l)	Relative Concentration C/C_∞^+
1	117.88	50	150	0:5	103	0.15
				0:30	470	0.71
				0:40	461	0.69
				0:50	555	0.83
				1:00	536	0.80
				1:15	559	0.84
				1:30	555	0.83
				1:45	559	0.84
				2:00	578	0.87
				2:15	611	0.92
				3:00	616	0.92

$^+C_\infty$ = 667 mg/l

APPENDIX A4

COLUMN LEACH TEST RESULTS

Table A4.1. Column leach test #1 (Aluminum oxide particles).

Sample #	Time (hrs)	Sample Volume (ml)	Cumul. Volume (ml)	Flow Rate (ml/hr)	Pore Volumes of inflow	Volume of Titrant (ml)	Cl Conc. (mg/l)	Rel. Conc.
Start	0.0							
B.T.	2.833				0.624			
1A	2.922	25	25		0.659			
1B	3.177	100	125	391	0.700	111.8	532	1.000
2A	3.241	25	150					
2B	3.496	100	250	393	0.775	108.6	517	0.972
3A	3.558	25	275					
3B	3.816	100	375	389	0.851	105.6	502	0.944
4A	3.879	25	400					
4B	4.137	100	500	388	0.926	103.0	490	0.921
5A	4.200	25	525					
5B	4.454	100	625	393	1.002	54.6	258	0.485
6A	4.517	25	650					
6B	4.776	100	750	386	1.077	16.4	76	0.143
7A	4.851	30	780					
7B	5.110	100	880	385	1.156	5.6	24	0.045
8A	5.161	20	900					
8B	5.433	100	1000		1.229	2.0	7	0.013
9A	5.483	25	1025					
9B	5.733	100	1125		1.304	2.0	7	0.013
10A	5.807	25	1150					
10B	6.058	100	1250		1.380	0.8	1	0.002
11	6.320	100	1350		1.440	0.8	1	0.002
12	6.574	100	1450	394	1.501	0.8	1	0.002
13	6.840	100	1550		1.561	0.8	1	0.002
14	7.093	100	1650	396	1.622	0.8	1	0.002

B.T. = Breakthrough

Table A4.2. Column leach test #2 (SiO_2 particles a=0.035cm).

Sample #	Time (hrs)	Sample Volume (ml)	Cumul. Volume (ml)	Flow Rate (l/hr)	Pore Volumes of Inflow (ml)	Volume of Titrant (ml)	Cl Conc. (mg/l)	Rel. Conc. C/C_m^+
Start	0.0							
B.T.	0.047				0.605			
1	0.056	50.0	50.0	5.62	0.675	88.4	900	0.882
2	0.065	50.0	100.0	5.81	0.814	66.6	678	0.665
3	0.073	50.0	150.0	6.00	0.953	48.8	496	0.486
4	0.081	51.5	201.5	6.39	1.095	34.6	341	0.334
5	0.089	52.0	253.5	6.24	1.239	22.7	221	0.217
6	0.098	51.5	305.0	5.79	1.383	14.5	142	0.139
7	0.107	51.0	356.0	6.12	1.526	8.6	84	0.082
8	0.115	51.5	407.5	6.18	1.668	5.0	48	0.047
9	0.123	51.5	459.0	6.39	1.812	3.2	30	0.029
10	0.132	52.0	511.0	5.85	1.956	2.0	18	0.018
11	0.140	52.0	563.0	6.45	2.101	1.1	9	0.009
12	0.149	51.0	614.0	5.92	2.244			
13	0.157	52.0	666.0	6.24	2.388	0.7	4.5	0.004
14	0.165	51.0	770.0	6.12	2.531			
15	0.174	51.0	768.0	5.92				
16	0.183	51.0	819.0	5.56				
17	0.191	50.0	869.0	6.00				
18	0.200	51.0	920.0	5.92				
	Average Flow Rate			6.03				

^+C_m = 1020 mg/l.

Table A4.3. Column leach test #5 (SiO_2 particles, a = 0.055 cm).

Sample #	Time (hrs)	Sample Volume (ml)	Cumul. Volume (ml)	Flow Rate (l/hr)	Pore Volumes of Inflow (ml)	Volume of Titrant (ml)	Cl Conc. (mg/l)	Rel. Conc. C/C_m^+
Start	0.00							
B.T.	0.113				0.513			
1	0.124	100	100	9.0	0.536	97.6	973	0.990
2	0.134	100	200		0.583	95.6	953	0.969
3	0.144	100	300	9.47	0.630	93.0	927	0.943
4	0.155	100	400		0.687	89.6	893	0.908
5	0.164	100	500		0.725	84.2	839	0.854
6	0.176	100	600		0.772	77.5	772	0.785
7	0.17	100	700	9.47	0.819	71.0	707	0.719
8	0.197	100	800		0.866	63.4	631	0.642
9	0.208	100	900	9.24	0.913	57.1	568	0.578
10	0.218	100	1000		0.960	50.9	506	0.515
11	0.229	100	1100		1.007	44.3	440	0.448
12	0.239	100	1200	9.48	1.054	37.7	374	0.380
13	0.249	100	1300		1.101	31.9	316	0.321
14	0.260	100	1400		1.148	27.4	271	0.276
15	0.270	100	1500		1.195	22.8	225	0.229
16	0.281	100	1600		1.242	20.0	197	0.200
17	0.291	100	1700		1.289	15.7	154	0.157
18	0.302	100	1800		1.336	12.6	123	0.125
19	0.312	100	1900	9.72	1.383	11.0	107	0.109
20	0.323	100	2000		1.430	7.5	72	0.073
21	0.333	100	2100		1.477	13.8	67	0.068
22	0.343	100	2200		1.524	11.2	53	0.054
23	0.354	100	2300	9.24	1.571	9.0	42	0.043
24	0.364	100	2400		1.618	7.1	33	0.034
25	0.375	100	2500		1.665	5.9	27	0.027
26	0.396	200	2700	9.48	1.736	4.2	18	0.018
27	0.417	200	2900		1.830	3.0	12	0.012
28	0.437	200	3100	9.48	1.924	2.3	9	0.009

^+C_m = 983 mg/l.

Table A4.4. Column leach test #6 (SiO_2 particles, a = 0.055 cm).

Sample #	Time (hrs)	Sample Volume (ml)	Cumul. Volume (ml)	Flow Rate (l/hr)	Pore Volumes of Inflow (ml)	Volume of Titrant (ml)	Cl Conc. (mg/l)	Rel. Conc. C/C_m +
Start	0.00							
B.T.	0.548				0.538			
1	0.566	25	25		0.544	54.9	1178	1.00
2	0.625	100	105					
3	0.83	100	225		0.615	121.6	1210	1.00
4	0.742	100	325	1.68				
5	0.801	100	425	1.68	0.709	111.0	1107	0.915
6	0.859	100	525	1.68	0.757	104.0	1037	0.857
7		100	625					
8		100	725					
9	1.032	100	825	1.74	0.899	77.0	767	0.634
10	1.088	100	925	1.80	0.947	67.0	667	0.551
11	1.144	100	1025	1.80				
12	1.200	100	1125	1.80	1.041	43.6	433	0.358
13	1.258	100	1225					
14	1.314	100	1325		1.136	24.6	243	0.201
15	1.371	100	1425					
16		100	1525		1.234	12.2	119	0.098
17		100	1625					
18	1.549	100	1725		1.329	7.3	70	0.058
19		100	1825					
20	1.656	100	1925		1.424	2.8	25	0.021
21	1.712	100	2025	1.78				
22	1.764	100	2125	1.91	1.519	3.2	13	0.10
23	1.817	100	2225	1.90				
24	1.871	100	2325	1.87	1.613	2.0	7	0.006
	Average Flow Rate			1.80				

+C_m = 1210 mg/l.

Table A4.5. Column leach tests (oil shales).

Sample (Bulk Density)	Pore Volumes (Influent)	Concentration (mg/l)	Relative Concentration
OS1 (1.25 gm/cm^3)	0.610	2270	1.000
	0.940	700	0.308
	1.390	280	0.123
	1.840	130	0.057
	2.500	30	0.013
	2.950	19	0.008
OS2 (1.36 gm/cm^3)	0.534	2380	1.000
	0.894	1150	0.483
	1.264	410	0.172
	1.614	110	0.046
	1.964	8	0.003
	2.264	6	0.003
OS3 (1.52 gm/cm^3)	0.402	2170	1.000
	0.832	1440	0.664
	1.242	370	0.171
	1.812	49	0.023
	2.022	44	0.020
	2.362	27	0.012

APPENDIX A5

COMPUTER PROGRAM

SOLUTION 1 INPUT VARIABLES LIST
LISTING
PRINTOUT

SOLUTION 2 INPUT VARIABLES LIST
LISTING

SOLUTION 3 INPUT VARIABLES LIST
LISTING

INPUT PARAMETERS FOR MODEL 1

FREE FORMAT

LINE	VARIABLE	DESCRIPTION
1	TITLE	NAME OF TEST
2	RIM	MICRO SPACE RETARDATION FACTOR
	RM	MACRO SPACE RETARDATION FACTOR
	THIM	MICRO SPACE WATER CONTENT
	THM	MACRO SPACE WATER CONTENT
	RAD	EFFECTIVE PARTICLE RADIUS
	Q	FLOW RATE
	S	SURFACE AREA 3*THIM/RAD
3	L	COLUMN LENGTH
	VM	DARCY VELOVITY
	DA	MICRO SPACE DIFFUSION COEFFICIENT
	DM	MACRO SPACE DISPERSION COEFFICIENT
	CI	INITIAL CONCENTRATION
	CO	INLFLOW CONCENTRATION
	AREA	AREA OF COLUMN
	PVM	MAX. VALUE OF PORE VOLUMES
4	DELT	TIME STEP
	DEL	DIVISIONS FOR INTEGRAND LAMDA
	NP	NUMBER OF POINTS FOR INTEGRATION IN ETA
	NP2	NUMBER OF ITERATIONS TO INCLUDE IN LAMD
	TOL	CUT OFF TOLERANCE FOR INTEGRATION LAMDA
	ETAM	MINIMUM VALUE FOR ETA
	TOLD	TOLRENACE FOR ENDING LAMDA ITERATIONS
	EM	MAXIMUM VALUE FOR ETA

```
$NOFLOATCALLS
$STORAGE:2
C ********************************************************************
C *                                                                  *
C *   CONCENTRATION BREAKTHROUGH CURVE WITH MICRO-PORE DIFFUSION     *
C *   SPHERICAL PARTICLES.                                           *
C *   MODEL 1                                                        *
C *                                                                  *
C ********************************************************************

      PROGRAM CONC
      IMPLICIT REAL*8(A-H,O-Z)
      REAL*8 L,LAM,LIMA,LIMB,LIMEA,LIMEB
      CHARACTER* 50 TITLE
C
C  OPEN FILES
C
      OPEN(5,FILE='CONC.DATA')
      OPEN(6,FILE='CONC.OUT')
      OPEN(7,FILE='PLOT.IN')
      READ(5,*) TITLE
      WRITE(6,1001) TITLE
C
C READ VARIABLES
C
      READ(5,*) RIM,RM,THIM,THM,RAD,Q,S
      READ(5,*) L,VM,DA,DM,CI,CO,AREA,PVM
      READ(5,*) DELT,DEL,NP,NP2,TOL,ETAM,TOLD,EM
      WRITE(6,1002) RIM,RM,THIM,THM,RAD,Q,S
      WRITE(6,1003) L,VM,DA,DM,CI,CO
C
C  ==================================================
C CALCULATE DOUBLE INTEGRAND
C ================================================
C
      PI=3.141592654
      TIME=0.0
      NDIV=INT((PVM*L/(DELT*VM))*(1+THIM/THM)+1)
      P=VM*L/DM
      G=S*DA*(L**2)/(THM*DM)
      S=S/RM
      VM=VM/RM
      DM=DM/RM
      WRITE(6,1004) P,G
      WRITE(7,1006) NDIV
      DO 7 I=1,NDIV
      ARGM=(EM/2.+P/4.-0.5*DSQRT(((EM+P/2.)**2)-((P/2.)**2-G/RAD)))
      IF(ARGM.LT.0.0) THEN
      EMIN=ETAM
      GOTO 8
      ENDIF
      EMIN=DSQRT(ARGM)
    8 EMAX=DSQRT(EM/2.+P/4.+0.5*DSQRT(((EM+P/2.)**2)-((P/2.)**2-G/RAD)))
      DELE=(EMAX-EMIN)/(NP-1)
      NQ=NP
      TIME=TIME+DELT
      PV=VM*RM*TIME*THM/(L*(THM+THIM))
```

```
C
C  INITIALIZE
C
      IFLAG2=0
      IFLAG=0
      ETA=EMIN-DELE
    1 SUMT=0.0
C
C  INTEGRAL ETA
C
      DO 5 K=1,NQ
      SUML=0.0
      LAM=0.0
      IFLAG=0
      ETA=ETA+DELE
      EM=EMAX+DELE
      IF(ETA.GT.EM) GOTO 6
C
C  INTEGRAL LAMDA
C
    2 LAM=LAM+DEL
      T=TIME-(1./DM)*(L/(2.*ETA))**2
      IF(T.LT.0.0) THEN
      NQ=NP2
      ETA=L/2*DSQRT(1./(TIME*DM))
      IF(IFLAG2.EQ.0) DELE=((EMAX-ETA)/(NQ-1))
      IFLAG2=1
      GOTO 1
      ENDIF
      THETA=RAD*LAM/DSQRT(DA)
      IF(THETA.GT.600.) THETA=600.
      PS1=(DSINH(THETA)-DSIN(THETA))/(DCOSH(THETA)-DCOS(THETA))
      PS2=(DSINH(THETA)+DSIN(THETA))/(DCOSH(THETA)-DCOS(THETA))
      BETA=1./(4.*ETA**2)
      TRIG1=DSIN(((LAM**2.)*T/2.)-(BETA*G*LAM*PS1)/(2.*DSQRT(DA)))
      TRIG2=DSIN(-BETA*G*LAM*PS1/(2.*DSQRT(DA)))
      TRIG=TRIG1-TRIG2
      A2=(-BETA*G*LAM*PS2/(2.*DSQRT(DA)))
      ARG1=(BETA*G/RAD)-(BETA*(P**2)/4.)-(ETA**2)+P/2.+A2
      SUM=DEXP(ARG1)
      SUM=(DEXP(ARG1))*TRIG/LAM
      SUML=SUML+SUM
      ITOLD=INT(TOLD)
      SUMF=SUMF+ABS(SUM)
      IF(IFLAG.EQ.(ITOLD+1)) THEN
      IF((SUMF/TOLD).LT.TOL) GOTO 3
      SUMF=0.0
      IFLAG=0
      ENDIF
      IFLAG=IFLAG+1
      GOTO 2
    3 WRITE(*,1007) TIME,ETA,LAM,SUM,SUML
      SUMT=SUMT+SUML*DEL*DELE
    5 CONTINUE
    6 CON=(CO-CI)*(4.*SUMT/PI**1.5)+CI
      CONCR=CON/CI
      WRITE(7,1009) PV.CONCR
      WRITE(6,1005) TIME,CON,PV,CONCR
      WRITE(*,1005) TIME,CON,PV,CONCR
    7 CONTINUE
```

```
C
C FORMAT
C
 1001 FORMAT(1H1,10X,68(1H*)/11X,1H*,66X,1H*/11X,1H*,4X,'BREAKTHROUGH '
     1'CURVE WITH MICRO-PORE DIFFUSION.',17X,1H*/11X,1H*,66X,1H*/11X,
     21H*,,4X,'SPHERICAL PARTICLES',43X,1H*/11X,1H*,66X,1H*/11X,1H*,
     366X,1H*/11X,1H*,4X,A50,12X,1H*/11X,68(1H*))
 1002 FORMAT(//11X,'INPUT PARAMETERS'/11X,16(1H=)//11X,'RIM=',F12.4,15X
     1,'RM=',F12.4/11X,'THIM=',F11.4,14X,'THM=',F12.4/11X,'RAD=',F12.4,
     216X,'Q=',F12.4,/11X,'S.AREA=',F9.4)
 1003 FORMAT(/11X,'LENGTH=',F12.4/11X,'PORE VEL.=',F9.4/11X,'DA=',
     1F12.4/11X,'DM=',F12.4/11X,'CI=',F12.4/11X,'CO=',F12.4)
 1004 FORMAT(//11X,'CALCULATED PARAMETERS'/11X,21(1H=)//11X,'P= ',
     1F12.4,/11X,'GAMMA=',F9.4///17X,'TIME',7X,'CONCEN.',4X,1H*,6X,
     2'PORE-VOLUME',6X,'REL. CONCEN.'//)
     2'TIME',7X,'CONCEN.',4X,1H*,6X,'PORE-VOLUME',6X,'REL. CONCEN.'//)
 1005 FORMAT(4X,2(4X,F12.4),3X,1H*,2(4X,F12.4))
 1006 FORMAT(I5)
 1007 FORMAT(2X,'T ',F5.2,2X,'ETA',F8.3,2X,'LAM',F8.3,2X,
     1'SUM',F10.6,2X,'SUML',F10.4)
 1008 FORMAT(4X,'ETA=',F5.3,2X,'SUML=',E12.4,2X,'ARG1=',F10.5,
     12X,'SUM=',E12.4,'SUML',F8.5)
 1009 FORMAT(2(2X,F12.4))
 1011 FORMAT(2X,'A2=',E12.4,'ARG1=',E12.4,'PS2=',E12.4)
      STOP
      END
```

```
***********************************************************************
*                                                                     *
*    BREAKTHROUGH CURVE WITH MICRO-PORE DIFFUSION.                    *
*                                                                     *
*    SPHERICAL PARTICLES                                              *
*                                                                     *
*                                                                     *
*     CURVE 3                                                         *
***********************************************************************


INPUT PARAMETERS
================

RIM=      1.0000                RM=       1.0000
THIM=      .4000               THM=        .4000
RAD=       .0450                 Q=      12.0000
S.AREA=  26.8000

LENGTH=     30.0000
PORE VEL.=  30.0000
DA=       .0100
DM=     30.0000
CI=   1000.0000
CO=       .0000


CALCULATED PARAMETERS
=====================

P=      30.0000
GAMMA=  20.1000

      TIME       CONCEN.     *      PORE-VOLUME     REL. CONCEN.


    .5000        999.9986    *           .2500          1.0000
   1.0000        992.1216    *           .5000           .9921
   1.5000        827.9463    *           .7500           .8279
   2.0000        454.7604    *          1.0000           .4548
   2.5000        170.7357    *          1.2500           .1707
   3.0000         49.2857    *          1.5000           .0493
   3.5000         11.6891    *          1.7500           .0117
   4.0000          2.7646    *          2.0000           .0028
   4.5000           .6485    *          2.2500           .0006
   5.0000           .1462    *          2.5000           .0001
```

INPUT PARAMETERS FOR MODEL 2

FREE FORMAT

LINE	VARIABLE	DESCRIPTION
1	TITLE	NAME OF TEST
2	RIM	MICRO SPACE RETARDATION FACTOR
	RM	MACRO SPACE RETARDATION FACTOR
	THIM	MICRO SPACE WATER CONTENT
	THM	MACRO SPACE WATER CONTENT
	RAD	EFFECTIVE PARTICLE RADIUS
	Q	FLOW RATE
3	L	COLUMN LENGTH
	VM	DARCY VELOVITY
	DA	MICRO SPACE DIFFUSION COEFFICIENT
	DM	MACRO SPACE DISPERSION COEFFICIENT
	CI	INITIAL CONCENTRATION
	CO	INLFLOW CONCENTRATION
4	DELT	TIME STEP
	DEL	DIVISIONS FOR INTEGRAND LAMDA
	TOL	CUT OFF TOLERANCE FOR INTEGRATION LAMDA

```
C **********************************************************************
C *                                                                    *
C *   CONCENTRATION BREAKTHROUGH CURVE WITH MICRO-PORE DIFFUSION       *
C *   SPHERICAL PARTICLES.                                             *
C *   MODEL 2                                                          *
C **********************************************************************

      PROGRAM CONC
      IMPLICIT REAL*8(A-H,O-Z)
      REAL*8 L,LAM,LIMA,LIMB
      CHARACTER* 50 TITLE
      DIMENSION X(20),H(20)
C
C  READ GAUSS QUAD POINTS
C
      OPEN(4,FILE='QUAD')
      OPEN(5,FILE='CONC.DATA')
      OPEN(6,FILE='CONC.OUT')
      OPEN(7,FILE='PLOT.IN')
      READ(4,*) NQ.(X(I),H(I),I=1,NQ)
      READ(5,*) TITLE
      WRITE(6,1001) TITLE
C
C READ VARIABLES
C
      READ(5,*) RIM,RM,THIM,THM,RAD,Q
      READ(5,*) L,VM,DA.DM,CI,CO
      READ(5,*) DELT,DEL,TOL
      WRITE(6,1002) RIM,RM,THIM,THM,RAD,Q
      WRITE(6,1003) L,VM,DA,DM,CI,CO
C
C  ==================================================
C CALCULATE INTEGRAND
C ================================================
C
      PI=3.141592654
      T=0.0
      NDIV=INT((2.5/DELT)+1)
      P=VM*L/DM
      G=DA*(THIM+THM)*L/((RAD**2)*Q*RIM)
      B=THM*RM/((THM*RM)+(THIM*RIM))
      R=((THIM*RIM)+(THM*RM))/(THM+THIM)
      WRITE(6,1004) P,G,B,R
      WRITE(7,1006) NDIV
      DO 7 J=1,NDIV
      T=T+DELT
      TIME=T*(THIM+THM)*L/Q
```

```
C
C  SET LAMDA
C
      IFLAG=0
      TERMP=0.0
      TERMN=0.0
      LIMA=0.0
      LIMB=DEL
      SUMT=0.0
    1 SUM=0.0
      DO 2 I=1,NQ
      LAM=(LIMB-LIMA)*(X(I)/2)+(LIMA+LIMB)/2
      PS1=3*LAM*(DSINH(2*LAM)+DSIN(2*LAM))/(DCOSH(2*LAM)-DSIN(2*LAM))
      PS1=PS1-3.
      PS2=3*LAM*(DSINH(2*LAM)-DSIN(2*LAM))/(DCOSH(2*LAM)-DCOS(2*LAM))
      OM1=((P**2)/4)+G*P*(1-B)*R*PS1
      OM2=(2*G*P*B*R*(LAM**2))+(G*P*(1-B)*R*PS2)
      RP=DSQRT((OM1**2)+(OM2**2))
      ZP=DSQRT(0.5*(RP+OM1))
      ZM=DSQRT(0.5*(RP-OM1))
    2 SUM=SUM+(H(I)/LAM)*(EXP((P/2)-ZP))*DSIN(2*G*(LAM**2)*T-ZM)*DEL/2
      IF (SUM.LT.0) GOTO 4
      TERMP=TERMP+SUM
      SUMT=SUMT+SUM
      IF (TERMN.EQ.0.0) GOTO 3
      IF (IFLAG.EQ.1) GOTO 3
      IF (ABS(TERMN/SUMT).LT.TOL) GOTO 6
      IFLAG=1
      TERMN=0.0
    3 LIMA=LIMB
      LIMB=LIMB+DEL
      GOTO 1
    4 TERMN=TERMN+SUM
      SUMT=SUMT+SUM
      IF (TERMP.EQ.0.0) GOTO 3
      IF(IFLAG.EQ.-1) GOTO 3
      IF(ABS(TERMP/SUMT).LT.TOL) GOTO 6
      IFLAG=-1
      TERMP=0.0
      GOTO 3
    6 CON=(CO-CI)*(0.5+2*SUMT/PI)+CI
      CONCR=(0.5+2*SUMT/PI)*((CO-CI)/CI)+1
      WRITE(7,1007) T,CONCR
    7 WRITE(6,1005) TIME,CON,T,CONCR
C
C FORMAT
C
 1001 FORMAT(1H1,10X,68(1H*)/11X,1H*,66X,1H*/11X,1H*,4X,'BREAKTHROUGH '
     1'CURVE WITH MICRO-PORE DIFFUSION.',17X,1H*/11X,1H*,66X,1H*/11X,
     21H*,,4X,'SPHERICAL PARTICLES',43X,1H*/11X,1H*,66X,1H*/11X,1H*,
     366X,1H*/11X,1H*,4X,A50,12X,1H*/11X,68(1H*))
 1002 FORMAT(//11X,'INPUT PARAMETERS'/11X,16(1H=)//11X,'RIM=',F12.4,15X
     1,'RM=',F12.4/11X,'THIM=',F11.4,14X,'THM=',F12.4/11X,'RAD=',F12.4,
     216X,'Q=',F12.4)
 1003 FORMAT(/11X,'LENGTH=',F12.4/11X,'PORE VEL.=',F9.4/11X,'DA=',
     1F12.4/11X,'DM=',F12.4/11X,'CI=',F12.4/11X,'CO=',F12.4)
 1004 FORMAT(//11X,'CALCULATED PARAMETERS'/11X,21(1H=)//11X,'P=',F12.4
     1/11X,'GAMMA=',F8.4/11X,'BETA=',F9.4,/11X,'R=',F12.4///17X,
     2'TIME',7X,'CONCEN.',4X,1H*,6X,'PORE-VOLUME',6X,'REL. CONCEN.'//)
 1005 FORMAT(4X,2(4X,F12.4),3X,1H*,2(4X,F12.4))
 1006 FORMAT(I5)
 1007 FORMAT(F10.5,2X,F10.5)
      STOP
      END
```

INPUT PARAMETERS FOR MODEL 3

FREE FORMAT

LINE	VARIABLE	DESCRIPTION
1	TITLE	NAME OF TEST
2	RIM	MICRO SPACE RETARDATION FACTOR
	RM	MACRO SPACE RETARDATION FACTOR
	THT	TOTAL WATER CONTENT
	THM	MACRO SPACE WATER CONTENT
	THIM	MICRO SPACE WATER CONTENT
	Q	FLOW RATE
3	L	COLUMN LENGTH
	VM	DARCY VELOVITY
	DA	MICRO SPACE DIFFUSION COEFFICIENT
	DM	MACRO SPACE DISPERSION COEFFICIENT
	CI	INITIAL CONCENTRATION
	CO	INLFLOW CONCENTRATION
	AREA	AREA OF COLUMN
	PVM	MAXIMUM PORE VOLUMES
4	DELT	TIME STEP
	NDI	NUMBER OF DIVISIONS FOR INTEGRATION

```
C *********************************************************************
C *
C *   CONCENTRATION BREAKTHROUGH CURVE WITHOUT MICRO-PORE DIFFUSION   *
C *   SPHERICAL PARTICLES.                                            *
C *   MODEL 3                                                         *
C *                                                                   *
C *********************************************************************

      PROGRAM CONC
      IMPLICIT REAL*8(A-H,O-Z)
      REAL*8 L,LAM,LIMA,LIMB,LIMEA,LIMEB
      CHARACTER* 50 TITLE
C     DIMENSION X(20),H(20)
C
C  READ DATA
C
      OPEN(5,FILE='CONCVN.DATA')
      OPEN(6,FILE='CONC.OUT')
      OPEN(7,FILE='PLOT.IN')
      READ(5,*) TITLE
      WRITE(6,1001) TITLE
C
C READ VARIABLES
C
      READ(5,*) RIM,RM,THT,THM,THI,Q
      READ(5,*) L,VM,DM,CI,CO,AREA,PVM
      READ(5,*) DELT,NDI
      WRITE(6,1002) RIM,RM,THT,THM,THI,Q
      WRITE(6,1003) L,VM,DM,CI,CO
C
C  ==================================================
C CALCULATE INTEGRAND
C ================================================
C
      PI=3.141592654
      TIME=DELT
      NDIV=INT((PVM*L/(DELT*VM))+1)
      P=VM*L/DM
      Q=VM*THM
      WRITE(6,1004) P
      WRITE(7,1006) NDIV
      DO 7 I=1,NDIV
      TLIM=(L-(VM*TIME))/(DSQRT(4.*TIME*DM))
      DELU=TLIM/NDI
      WRITE(*,*) TLIM,DELU
      SUM=0.0
      U=DELU/2.
      DO 1 J=1,NDI
      SUM=SUM+DEXP(-1.*(U**2))
      U=U+DELU
C     WRITE(*,*) SUM,U
    1 CONTINUE
      SUM=SUM*DELU*(1./DSQRT(PI))+0.5
      CON=CI*SUM
      CONCR=CON/CI
      PV=(VM*TIME)/(L)
      WRITE(7,1009) PV,CONCR
      WRITE(6,1005) TIME,CON,PV,CONCR
      WRITE(*,1005) TIME,CON,PV,CONCR
    7 TIME=TIME+DELT
```

```
C
C FORMAT
C
 1001 FORMAT(1H1,10X,68(1H*)/11X,1H*,66X,1H*/11X,1H*,4X,'BREAKTHROUGH
     1'CURVE WITH MICRO-PORE DIFFUSION.',17X,1H*/11X,1H*,66X,1H*/11X,
     21H*,,4X,'SPHERICAL PARTICLES',43X,1H*/11X,1H*,66X,1H*/11X,1H*,
     366X,1H*/11X,1H*,4X,A50,12X,1H*/11X,68(1H*))
 1002 FORMAT(//11X,'INPUT PARAMETERS'/11X,16(1H=)//11X,'RIM=',F12.4,15X
     1,'RM=',F12.4/11X,'THT= ',F11.4,14X,'THM=',F12.4/11X,'THI=',F12.4,
     216X,'Q=',F12.4)
 1003 FORMAT(/11X,'LENGTH=',F12.4/11X,'PORE VEL.=',F9.4/11X,
     1'DM=',F12.4/11X,'CI=',F12.4/11X,'CO=',F12.4)
 1004 FORMAT(//11X,'CALCULATED PARAMETERS'/11X,21(1H=)//11X,'P= ',
     1F12.4///17X,'TIME',7X,'CONCEN.',4X,1H*,6X,
     2'PORE-VOLUME',6X,'REL. CONCEN.'//)
     2'TIME',7X,'CONCEN.',4X,1H*,6X,'PORE-VOLUME',6X,'REL. CONCEN.'//)
 1005 FORMAT(4X,2(4X,F12.4),3X,1H*,2(4X,F12.4))
 1006 FORMAT(I5)
 1007 FORMAT(2X,'T ',F5.2,2X,'ETA',F8.3,2X,'LAM',F8.3,2X,
     1'SUM',F10.6,2X,'SUML',F10.4)
 1008 FORMAT(4X,'ETA=',F5.3,2X,'SUML=',E12.4,2X,'ARG1=',F10.5,
     12X,'SUM=',E12.4,'SUML',F8.5)
 1009 FORMAT(2(2X,F12.4))
 1011 FORMAT(2X,'A2=',E12.4,'ARG1=',E12.4,'PS2=',E12.4)
      STOP
      END
```